Agricultural and Forest Meteorology 252 (2018) 241–255

Contents lists available at ScienceDirect

Agricultural and Forest Meteorology

journal homepage: www.elsevier.com/locate/agrformet

Limitations to winter and spring photosynthesis of a Rocky Mountain subalpine forest

David R. Bowling[a,*], Barry A. Logan[b], Koen Hufkens[c], Donald M. Aubrecht[c], Andrew D. Richardson[c], Sean P. Burns[d,e], William R.L. Anderegg[a], Peter D. Blanken[d], David P. Eiriksson[f]

[a] Department of Biology, University of Utah, 257 South 1400 East, Salt Lake City, UT, 84112, United States
[b] Department of Biology, Bowdoin College, Brunswick, ME, 04011, United States
[c] Department of Organismic and Evolutionary Biology, Harvard University, Cambridge, MA, 02138, United States
[d] Department of Geography, University of Colorado, Boulder, CO, 80309, United States
[e] National Center for Atmospheric Research, Boulder, CO, 80301, United States
[f] Global Change and Sustainability Center, University of Utah, Salt Lake City, UT, 84112, United States

ARTICLE INFO

Keywords:
Conifer
Climate change
Xylem temperature
Pinus contorta
Abies lasiocarpa
Picea engelmanii

ABSTRACT

Temperate and boreal conifer forests are dormant for many months during the cold season. Climate change is altering the winter environment, with increased temperature, altered precipitation, and earlier snowmelt in many locations. If significant enough, these changes may alter patterns of dormancy and activity of evergreens. Here we studied the factors limiting photosynthetic activity of a high-elevation subalpine forest that has undergone substantial warming in recent decades. We tested the hypothesis that this warming has been significant enough to allow photosynthesis during sunny warm days in winter. Using thermal imagery, we found that foliage in winter was sometimes near the temperature optimum for photosynthesis, but no net carbon gain occurred for most of the cold season. Water transport was limited by blockage of sap transport by frozen boles, but not by frozen soils. Foliar carotenoid content was much higher during winter, driven largely by increases in the pool size of the photoprotective xanthophyll cycle. There was no seasonal change in chlorophyll or lutein content. Net carbon uptake began only as boles thawed, with no difference in timing among tree species, and the spring increase in canopy-level photosynthetic capacity occurred before sap transport was detected. The seasonality of gross primary productivity (GPP) was strongly linked to seasonality of xanthophyll cycle deepoxidation state in all species. Seasonality of GPP was detectable with two metrics of canopy color – the Green Chromatic Coordinate and Green-Red Vegetation Index (a proxy for the newly proposed MODIS-based chlorophyll/carotenoid index or CCI). Both indices were significantly correlated with GPP. Together these results indicate the potential for airborne or near-surface remote sensing of leaf color to serve as a metric of photosynthetic activity in evergreen forests, and to monitor physiological changes associated with the progression in and out of winter dormancy.

1. Introduction

The climate of seasonally snow-covered ecosystems is changing, affecting the seasonality of winter and the timing of biophysical events related to photosynthetic downregulation. In many locations, late winter air temperature is increasing (Kapnick and Hall, 2012; Pederson et al., 2013), total accumulations of snow are decreasing (Hamlet et al., 2005; Mote et al., 2005), relatively more winter precipitation falls as rain instead of snow (Knowles et al., 2006), and snowmelt occurs earlier (Clow, 2010; Stewart et al., 2005). Climate models indicate that these changes will continue (Brown and Mote, 2009; Nogués-Bravo et al., 2007; Scalzitti et al., 2016).

Evergreen plants in seasonally snow-covered locations endure the physiological stress of winter while still absorbing appreciable sunlight. Most undergo biochemical downregulation of photosynthesis that manifests as a decrease in photosynthetic capacity and alterations in pigment composition associated with photoprotection (Adams et al., 2004; Öquist and Huner, 2003; Verhoeven, 2014). Overwintering evergreens have been shown to utilize two forms of sustained thermal energy dissipation to cope with excess absorbed light, a rapidly-

* Corresponding author.
E-mail address: david.bowling@utah.edu (D.R. Bowling).

https://doi.org/10.1016/j.agrformet.2018.01.025
Received 27 February 2017; Received in revised form 21 December 2017; Accepted 18 January 2018

reversible form that is important when favorable temperature for photosynthesis may occur periodically, and a slowly-reversible form that is associated with more sustained downregulation of photosynthesis in colder climates (Verhoeven, 2014). Both forms involve xanthophyll cycle pigments, and may operate in synergy (Porcar-Castell, 2011). Despite this, some conifers maintain appreciable photosynthetic capacity in winter (Nippert et al., 2004; Schaberg et al., 1998; Schulze et al., 1967).

Physiological activity and phenology of plants are responding to the persistent changes in winter climate. The combination of decreasing snow cover and increasing air temperature has complex biophysical and biogeochemical effects on plants and soils (Brooks et al., 2011; Groffman et al., 2001; Kreyling, 2010). The phenology of small plants that spend winter under the snow is strongly altered by earlier snowmelt (Steltzer et al., 2009). Trees and shrubs that extend above the snowpack are responding to warming generally with earlier leaf expansion in spring and later senescence in autumn (Polgar and Primack, 2011). Spring greenup occurs earlier across the northern hemisphere (Barichivich et al., 2013; Piao et al., 2011). Earlier spring and later autumn influence annual gross primary productivity (GPP) and ecosystem respiration (R_{eco}) (Richardson et al., 2010, 2009). Thus, the carbon cycle of seasonally snow-covered biomes is being modified on a large scale as climate changes, and this is detectable in the amplitude and timing of the seasonal cycle of atmospheric CO_2 (Forkel et al., 2016).

The factors governing the transition from the downregulated state of photosynthesis (winter dormancy) to spring activity are complex. Rather than an on-off switch, release from dormancy is intermittent with periods of activity based on re-establishment of photosynthetic metabolism and variability of weather (Ensminger et al., 2004; Sevanto et al., 2006; Turcotte et al., 2009). In some trees, photosynthetic activity can respond opportunistically to favorable periods during the otherwise cold season (Ensminger et al., 2004) if plants are able to maintain some photosynthetic capacity and water is available (Kolari et al., 2014; Nippert et al., 2004). Earlier snowmelt potentially leads to earlier phenological development and physiological activity of plants, but alternatively if air temperature is low during melt then carbon metabolism can be dramatically limited (Huxman et al., 2003; Winchell et al., 2016). Thus, as the climate warms, some plants may encounter a new regime where novel environmental conditions (combinations of photoperiod, air/soil temperature, snow cover, and water availability) result in physiological stress. The carbon cycle implications of such change remain highly uncertain.

For these reasons, we were motivated to examine the cold season carbon cycling of a high elevation coniferous forest in Colorado. This subalpine forest has undergone significant recent climate warming. Mean annual temperature has increased by ~1.1 °C/decade (Clow, 2010) to 2.7 °C in the 2000s (Mitton and Ferrenberg, 2012). Air temperature in each month February through May has significantly increased (McGuire et al., 2012), and April-May temperature has increased by 0.7 °C/decade (Kittel et al., 2015). Mean annual precipitation is about 800 mm, with a majority falling as snow. Total cold season precipitation has not changed, but the total now includes considerably more precipitation in April that used to occur in May (Kittel et al., 2015). This, combined with warmer cold season air temperature and thus higher convective heat flux during snowmelt when some bare ground is exposed, will likely lead to consistently earlier snowmelt. In most mountain basins of this region, total snow water equivalent is decreasing and snowmelt begins earlier than in recent decades (Clow, 2010).

Our primary objective was to evaluate the hypothesis that the climate has warmed sufficiently to allow the conifers at the Niwot Ridge forest to photosynthesize during favorable warm sunny periods in winter. A secondary objective was to determine if visible-wavelength imagery could be used to identify periods of activity and dormancy. We integrate data from a variety of sources, including a combination of microclimatic and micrometeorological observations, visible-wavelength and thermal imagery, and leaf-level pigment analyses. We anticipated that physiological differences might occur between co-dominant tree species in cold season activity or release from dormancy, and expected that initiation of sap transport would occur before net carbon uptake was detectable.

2. Material and methods

2.1. Study location

This study was conducted at the subalpine forest of the Niwot Ridge AmeriFlux Core site (US-NR1) in the Rocky Mountains of Colorado, U.S.A. (40.03°N, 105.55°W, 3050 m elevation). The flux tower is surrounded by a mix of evergreen needleleaf species: lodgepole pine (*Pinus contorta* Douglas ex Loudon), Engelmann spruce (*Picea engelmannii* Parry ex Engelm.), and subalpine fir (*Abies lasiocarpa* (Hook.) Nutt.). Average tree height and leaf area index are 12–13 m and 3.8–4.2 m^2 m^{-2}, respectively, and the stem density is ~4000 stems ha^{-1}. This high elevation forest experiences cold winters with a persistent snowpack from October-November to May/June. Extensive site details are available in other publications (Burns et al., 2015; Monson et al., 2002). For the present study, observations are reported over a 1-yr period centered on the winter of 2015/2016. The study winter was a bit warmer than the monthly averages of 15 years preceding it (2000–2014) during January and February, but cooler than average for other months (Table 1). Peak snow water equivalent during the study winter was 419 mm, the 5th largest snowpack since the 2000 water year.

2.2. Meteorological parameters and carbon fluxes

Environmental conditions were monitored to examine their influence on forest activity and dormancy. Wind, down-welling photosynthetically active solar radiation (PAR), and net radiation (4-component) were measured above canopy, and air temperature both above canopy (21.5 m) and below (2 m), using standard sensors described in Burns et al. (2015). Soil moisture was measured with water content reflectometers (CS616, Campbell Scientific). Soil temperature was measured at 5 cm depth in mineral soil using a thermistor probe (CS107, Campbell Scientific). Snow water equivalent (SWE) data from a site 400 m distant from the flux tower were obtained from USDA/Natural Resources Conservation Service Snow Telemetry Network (site Niwot).

Net ecosystem exchange (NEE) of carbon dioxide was measured at 21.5 m above ground using the eddy covariance method, accounting for

Table 1
Comparison of air temperature during selected months between the study winter (2015/16) and the 15 years preceding it (2000–2014). Shown are the 15-year mean, standard deviation (SD), the maximum and minimum mean monthly temperature for each month, and the monthly means for the 2015/16 winter. The 2015/16 data are compared to the 15-year records and ranked in the last column.

month	15-year record				2015/16	
	mean (°C)	SD (°C)	max (°C)	min (°C)	mean (°C)	2015/16 rank
November	−2.5	2.0	0.2	−7.1	−3.5	5th warmest
December	−6.7	1.6	−4.5	−10.4	−7.1	10th warmest
January	−6.4	1.5	−3.5	−9.3	−6.0	6th warmest
February	−7.1	1.5	−3.7	−9.0	−4.3	2nd warmest
March	−3.5	1.8	0.2	−5.9	−4.0	10th warmest
April	−0.2	1.7	2.4	−3.5	−0.9	7th warmest

CO_2 storage within the canopy (Burns et al., 2015). The fluxes of GPP and R_{eco} were partitioned from NEE using either soil or air temperature (main paper and supplemental material, respectively) using the method of Reichstein et al. (2005) via the online tool at http://www.bgc-jena.mpg.de/~MDIwork/eddyproc/index.php.

2.3. Thermal dissipation sap flux

To detect the presence of cold season water transport by individual trees, sap flux density was measured using the thermal dissipation (TD) method (Granier, 1987, 1985). Two trees close to the tower were measured per species (pine, spruce, fir), with homemade sensors, installed at breast height on the north sides of the boles and covered with reflective insulation. Sensors penetrated 21 mm into the xylem. Bole diameters at breast height (DBH) ranged from 14 to 41 cm. Laboratory and field tests have shown that this method reliably detects water movement in tree boles when it occurs in winter (Chan and Bowling, 2017). We are less confident in the actual magnitude of sap flux density determined using TD under cold and low flow conditions, so data are reported as raw voltages from sensor pairs, and as relative sap flux density (on a 0 to 1 scale, with 0 being no transport and 1 the maximum measured for a sensor pair). Sap flux density was calculated using the standard Granier equation with a changing baseline prior to normalizing (Chan and Bowling, 2017). Sapwood area and depth were not measured. Sapwood depth for the trees at Niwot Ridge is typically > 30 mm for fir and deeper for pine and spruce (Jia Hu and David J. P. Moore, personal communication, Hu et al., 2010; Moore et al., 2008), so the sap flux and bole temperature probes (described below) were well surrounded by hydro-active xylem.

2.4. Light and temperature response of ecosystem fluxes

To examine the seasonality of photosynthetic activity, the environmental dependence of carbon and water fluxes was examined. The light (PAR) responses of sap flux density, NEE, and GPP were examined for periods of interest using nonlinear regressions. All daylight periods with thawed boles were combined during each period (we did not separate morning and afternoon). These were of the form $y = (ax)/(1 + bx)$ for sap flux and GPP, or $y = (ax)/(1 + bx) + c$ for NEE. The temperature (soil or air) responses of R_{eco} were examined using nonlinear regressions of the form $y = ae^{(bx)}$.

A seasonally varying index of canopy-level photosynthetic capacity (GPP_{sat}) was calculated for 10-day periods by first calculating the light response for GPP in each time period, then extracting the curve fit value at high PAR (1800 $\mu mol\, m^{-2}\, s^{-1}$). This index is illustrated with selected GPP light response curves in Fig. 5. The light level at which photosynthesis saturates will change seasonally, but choosing a constant PAR value provides for comparison of capacity across the annual cycle in a consistent fashion.

2.5. Bole temperature

The temperature of hydro-active xylem of tree boles (tree trunks) was monitored to evaluate blockage of water transport by ice. Bole temperature (at breast height) was measured using 20-gauge nickel-chromium/constantan (type E) thermocouples (FF-E-20-TWSH-SLE, Omega), selected for their low thermal conductivity. Sensors were inserted at 12 and 30 mm depths into xylem on the north sides of trees (1 per species), in autumn. Bole diameters at breast height were 20, 22, and 16 cm for pine, spruce, and fir trees, respectively. Sensors were sealed in place with epoxy, and cables were insulated with reflective foam and routed along the ground (under the snowpack) to prevent solar radiation artifacts. Tree trunks were not insulated, and different trees were used for the bole temperature and sap flux measurements. The presence of ice in the bole was determined from these data as described in Results.

2.6. Foliage temperature

Thermal infrared imaging was used to measure the temperature of individual tree crowns in the vegetation canopy following Aubrecht et al. (2016). Thermal images were recorded by an A655sc camera (FLIR Systems, Inc., 640 × 480 pixel resolution, 45° field of view, FOV) mounted near the top of the tower, pointed east and inclined about 30° below the horizon. Images were acquired every 5 min using FLIR's ExaminIR software, running on an industrial fanless computer (Neousys POC-100, Logic Supply) mounted in an enclosure on the tower. The crowns of trees instrumented with sap flux sensors were within the FOV of this camera, and the visible imaging camera (discussed below).

Supporting measurements for correcting and verifying the thermal images were made with instruments mounted in the immediate vicinity of the thermal camera. These included: a temperature/relative humidity probe (HMP35-C, Vaisala), three infrared radiometers pointed at vegetation within the FOV of the thermal camera (SI-121, Apogee, 18° half-angle FOV), and down-welling longwave radiation (CNR1, Kipp and Zonen) to calculate sky temperature. To verify temperature from the thermal images, a matte-black-painted copper plate (5.1 × 15.2 × 0.19 cm, emissivity = 0.985) was mounted on a boom in the FOV of the thermal camera. A copper-constantan thermocouple was affixed to the front of the plate with thermal epoxy and the plate temperature was recorded every 30 s. Camera-derived temperature of the plate was highly correlated with the independently measured temperature ($r^2 = 0.997$, linear regression, $p < 0.001$, *t*-test). The mean absolute difference (camera T - actual T) was -0.20 °C, variance = 0.29 $°C^2$, with root-mean-square error of 0.57 °C (n = 53,852).

Vegetation temperature was determined from thermal images following Aubrecht et al. (2016). Briefly, each image was paired with simultaneous meteorological data: air temperature, relative humidity, and apparent sky temperature. Combined with a distance-to-canopy map for each pixel in the image, vegetation emissivity (assumed 0.97), and models of atmospheric transmission, these data were used to calculate the thermal interference in the image caused by reflections of surroundings, attenuation of canopy temperature signal by moisture in the air, and re-radiation of thermal energy by moisture in the air. Corrections for these interferences were applied to each thermal image to arrive at the true vegetation temperature. Foliage temperature is reported as the mean temperature of pixels that correspond to individual tree crowns in each image. Each crown region of interest was determined manually, intentionally excluding stems due to their difference from leaf temperature (Kim et al., 2016), and used the same pixels for all analyzed images. The distance-to-canopy map was created using multiple color digital images and structure from motion software (PhotoScan, Agisoft LLC), as described in detail by Aubrecht et al. (2016). These corrections were not applied to the SI-121 radiometer data. The SI-121 data were cold-biased relative to those from the thermal images (mean difference −2.0 °C, standard deviation 1.6 °C, n = 38,091 for the data shown in Fig. 1d).

2.7. Visible imagery (PhenoCam)

Visible-wavelength digital imagery was used to assess possible color-based metrics of the seasonality of photosynthesis. Standard three-color (red-green-blue, RGB) images were recorded by a network-enabled camera (NetCam SC, StarDot Technologies). The camera was configured according to standard PhenoCam protocols (https://phenocam.sr.unh.edu/webcam/tools/, manuscript in preparation) and acquired images every 15 min between 0400 and 2300 local standard time. For a prescribed region within each image, we extracted the mean pixel value (digital number, DN) for each color channel (i.e. R_{DN}, G_{DN}, B_{DN}). Spectral response of the PhenoCam used is available at https://khufkens.github.io/phenocam-response-curves/. At half-maximum the approximate spectral ranges were: R_{DN}: 570–700 nm, peak at 600 nm,

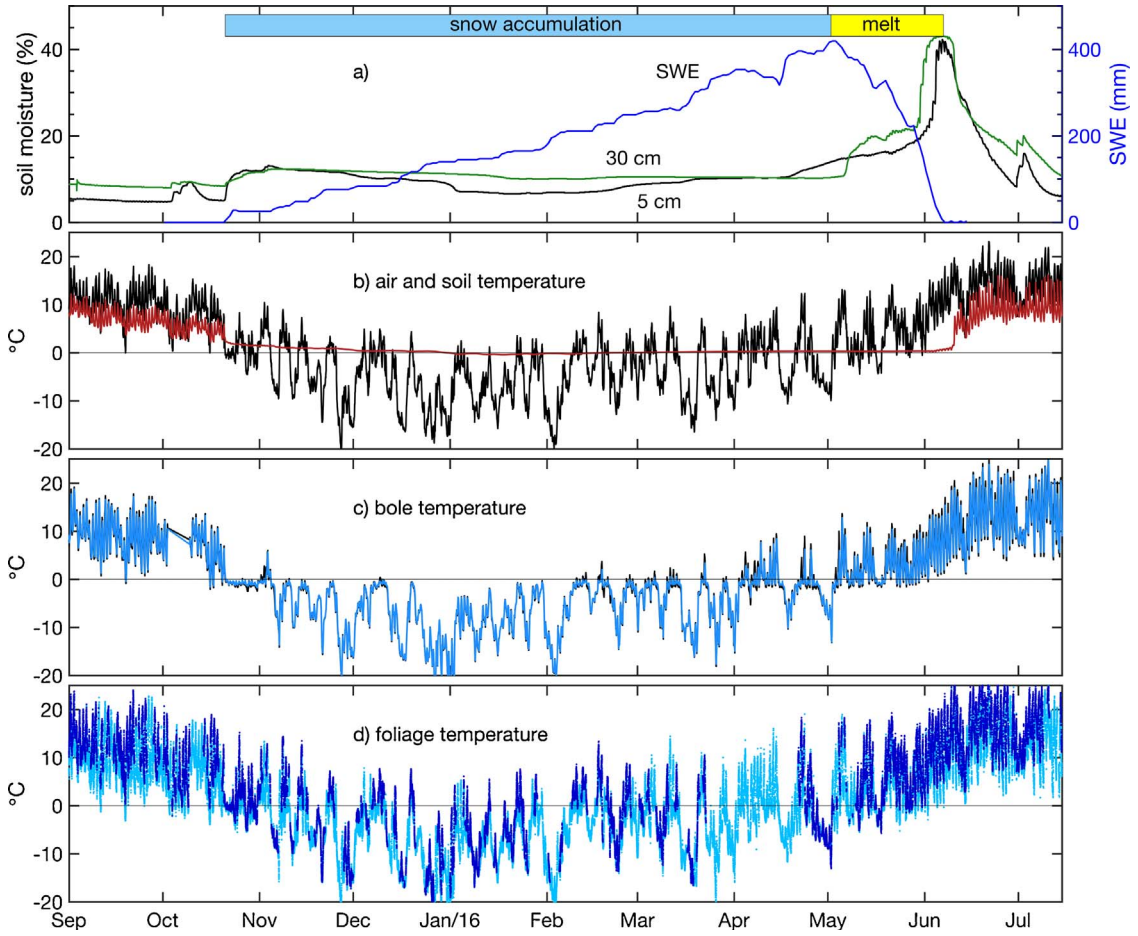

Fig. 1. Environmental conditions during the cold season of 2015/16 at the Niwot Ridge forest. a) Soil moisture (left axis) and snow water equivalent (SWE, right), with boxes indicating the periods of snow accumulation and melt, b) air (21m above ground) and soil (5 cm depth) temperature, c) spruce bole temperature at 12 mm (black) and 30 mm (blue) depth in xylem, and d) foliage temperature of spruce crown #3 measured with thermal infrared imaging (dark blue) and temperature of the overall canopy measured with a wide field of view infrared radiometer (light blue). Some data are missing in panel d) due to instrument failure.

G_{DN}: 490–580 nm, peak at 530 nm, and B_{DN}: 390–500 nm, peak at 450 nm.

From these data we derived 3-day composite values of the Green Chromatic Coordinate, G_{CC} (Motohka et al., 2010) and the Green-Red Vegetation Index, GRVI (Tucker, 1979). The indices were calculated as $G_{CC} = G_{DN}/(R_{DN}+G_{DN}+B_{DN})$, and $GRVI = (G_{DN}–R_{DN})/(G_{DN}+R_{DN})$. Previous work (Sonnentag et al., 2012) has shown that under adverse lighting and weather conditions (rain, clouds and snow), observed values of G_{CC} tend to be reduced relative to images recorded under sunny skies. For this reason, Sonnentag et al. (2012) proposed that the 90th percentile value of G_{CC}, calculated over a 3-day period, effectively minimized day-to-day variation due to exogenous factors by tracking the upper envelope of the data. We found a similar approach, but based on calculating the 10th percentile, was effective for GRVI. The 3-day data were then filtered with an iterative, spline-based smoothing algorithm. First, using a range of smoothing factors, we fit a family of cubic smoothing splines to each time series. We selected the optimal spline from within this family using the Bayesian Information Criterion balancing goodness-of-fit against model complexity to avoid over-fitting. Then, in an iterative process, we identified and flagged outliers more than 4 Laplace standard deviations (based on the first difference of the original time series) from the spline (Richardson and Hollinger, 2005).

In order to conduct certain analyses using data when the canopy was snow-free, the RGB images were analyzed to determine the presence of snow. We automated this procedure using methods based on recent advances in computer vision and artificial intelligence. Specifically, we used the Caffe deep learning framework (Jia et al., 2014) in conjunction with the Places205-AlexNet trained model (Zhou et al., 2014), to classify images. We used the classification tags “trees” and “snow” produced by the framework, and if the “snow” tag was more heavily weighted than the “trees” tag, the image was marked as “snowy canopy”. Informal validation of this method showed that this method successfully identified when snow was in the air or on the canopy, but did not mistakenly classify images when there was only snow on the ground. To determine when the thermal camera imagery may have been contaminated by snow, we assumed that snow on the canopy was possible only if the air temperature was below freezing. Then, we analyzed the seven RGB images recorded closest to each thermal camera image (within a 24 h window, but using RGB imagery only when the sun was above the horizon). If four or more of these seven images were marked as “snowy canopy”, then the thermal image was flagged as potentially snow-contaminated.

The G_{CC} and GRVI indices were compared to seasonality of solar forcing using the solar elevation angle above the southern horizon at solar noon, calculated from standard equations (Campbell and Norman, 1998).

2.8. Needle chlorophyll and carotenoid composition

Pigments in conifer needle (leaf) tissue were measured to evaluate seasonal adjustments associated with the downregulation of photosynthesis. Using a canopy access tower, sun-acclimated needles from the uppermost 1.5 m of the canopy were collected from one tree of each

Table 2
Temperature of tree crowns (mean of 6 individual crowns, 2 per species) measured via thermal imagery when foliage was snow-free, during different months. Shown are the monthly maximum and minimum, the mean and maximum daily range (difference between the daily maximum and minimum), the number of days above 0, 5, and 10 °C, and the data availability for all 5-min measurement periods in the month (with and without snow).

month	max (°C)	min (°C)	daily range (mean,°C)	daily range (max, °C)	n days > 0 °C	n days > 5 °C	n days > 10 °C	data coverage %
November	13.3	−15.0	8.7	16.2	11	8	4	57.2
December	6.4	−16.6	7.7	14.2	7	2	0	46.4
January	6.5	−20.8	9.2	19.0	7	2	0	55.9
February	11.8	−14.9	9.1	16.0	11	6	1	51.2
March	9.3	−14.4	8.8	15.9	7	5	0	34.9
April	17.5	−6.8	10.2	18.1	7	5	3	28.4

species ~biweekly between 15 August 2015 and 23 June 2016 (one to three replicate measurements were made per tree per collection date; error bars on figures depicting leaf pigment composition represent standard deviation). Needles were immediately wrapped in foil and immersed in liquid nitrogen within 10 min, and stored either in liquid nitrogen or a −80 °C freezer until extraction.

Needle chlorophylls and carotenoids were extracted according to a procedure modified from Adams and Demmig-Adams (1992). Approximately 25 mg of frozen needle tissue were ground for 4–6 min (sufficient to fully pulverize tissue by visual inspection) in 500 µl of ice-cold 80% acetone (v/v) using a high-energy ball mill (CertiPrep 8000D, Spex CertiPrep) equipped with sample containers modified to hold micro-centrifuge tubes. Samples were then spun in a refrigerated micro-centrifuge (3 °C) for five minutes at 14,000 rpm (18,188 g) and the supernatant collected. The pellet of cellular debris was then agitated in 200 µl of ice-cold 100% acetone. Centrifugation was repeated and the resultant supernatant was combined with that of the initial extraction. Re-extraction of the pellet was then repeated as above. The volume of each sample extract was determined using a graduated 1 mL syringe and the sample was passed through a 0.2 µm nylon syringe tip filter into a sealable amber vial and maintained at 0–4 °C until analysis (< 10 h).

Extracted chlorophylls and carotenoids were quantified using a liquid chromatograph with diode array detector (Agilent 1100, Agilent Technologies) set to record at 445 nm and a YMC Carotenoid C_{30} reverse phase column (5 µm particle size, 250 mm × 4.6 mm I.D.; YMC America) using a gradient method involving 1.5 min acetonitrile:methanol:water (86.4:10:3.6 (v/v)) followed by a linear gradient over the ensuing five minutes to a 4:1 mixture of methanol and hexanes, concluding with 8.5 min of the latter solvent (all at 2 ml/min). The mobile phases were composed of HPLC grade organic solvents (Pharmco-AAPER and Fisher Scientific) and 0.2 µm filtered type I deionized water. Pigments measured included chlorophyll A and B, violaxanthin, antheraxanthin, zeaxanthin, neoxanthin, lutein, and α- and β-carotene. Needle pigment contents are expressed as moles per unit fresh mass and as molar ratios (chlorophyll a/b and total chlorophyll/total carotenoid).

Pigment data may be found in the Supplementary Material.

2.9. Statistical analyses

Statistical analyses were performed to determine if differences existed in the response of fluxes to light and temperature, and to assess relationships between GPP_{sat}, xanthophyll cycle pigments, and the G_{CC} and GRVI indices. Light and temperature response curve fits (equations described above) and their 95% confidence bounds, during the four periods of interest, were generated using the Curve Fitting Toolbox of MATLAB R2016b (MathWorks, Natick, MA). Non-overlapping confidence bounds indicate significant differences ($p <= 0.05$). The GPP_{sat} was compared to the midday deepoxidation state of leaf xanthophyll pigments for each species, and the G_{CC} and GRVI indices using linear regression, and the null hypothesis (slope = 0) was examined using a *t*-test (with $p = 0.05$ the threshold for significance of non-zero slope).

3. Results

Environmental conditions during the study are shown in Fig. 1. Permanent snow cover was established in late October and continued to accumulate until peak SWE was reached in early May. Soil moisture under the snowpack was fairly constant, with late autumn conditions persisting until snowmelt events occurred in April and May. The first events led to a moderate increase in soil moisture, but major changes were delayed until the melt began in earnest a few weeks later. During the snow accumulation period, air temperature varied from -20 °C to + 13 °C, with many winter days above freezing. In contrast, soil temperature under the snowpack (5 cm soil depth) was nearly constant and above 0 °C (Fig. 1b), except for a few weeks in January when it reached a minimum of -0.4 °C. Deeper soils under the snowpack were always warmer than the 5 cm depth (data not shown).

The temperature of evergreen tree crowns during the cold season was highly variable (Fig. 1d, Table 2 - note these data were only when the canopy was free of snow). Minimum foliage temperature during the snow accumulation and melt periods was -20.8 °C, and maximum monthly temperature ranged from 6.4 (December), 11.8 (February) to 17.5 °C (April). The average daily range of temperature of tree crowns in each month was 8–10 °C (maximum - minimum over 24 h), with maximum daily ranges of 14-19 °C. In all winter months the foliage temperature was above 0 °C for 7–11 non-consecutive days, above 5 °C for 2–8 days, and in November, February, and April, above 10 °C. In general, during sunny days with no snow in the canopy, the foliage was always warmer than air by as much as 5 °C, especially when winds were light, but also during windy periods (Fig. 2). Air and foliage temperature both varied with weather events (Fig 1b, d) and with net radiation (Fig. 2). During the winter (February) there was little difference in foliage temperature between species (Supplemental Table S1). In June, fir crowns were generally warmer than those of pine and spruce, consistent with known differences in whole-tree transpiration rate for these species (Hu et al., 2010).

The frequent synoptic change in air temperature was associated with marked change in bole temperature throughout the winter, though buffered by phase changes of xylem sap. Xylem temperature in the boles (Fig. 1c) remained at or below 0 °C from late October through early February for all 3 tree species (only spruce shown, other species similar). In warm periods during February and March, there were brief excursions with xylem above 0 °C, then alternating sustained warm and cold periods in April. In April and May as air temperature warmed, the bole temperature displayed a well-bounded minimum around -2 °C, indicative of the liquid-ice phase transition region (Fig. 3).

Freezing of ice releases energy, and thawing of ice consumes energy, and these phase changes can be detected in woody tissue by comparing the difference in bole and air temperature as a function of bole temperature (Hadley, 2000; Mayr et al., 2006). Bivariate frequency distributions of the difference between bole and air temperature at 2 m (y-axis) versus bole temperature (x-axis) are plotted in Fig. 3. Data were combined for November 1–April 30 for each thermocouple separately, and used to determine the presence of ice in the boles as follows. Regions of high frequency of occurrence shown in the circle (Fig. 3a)

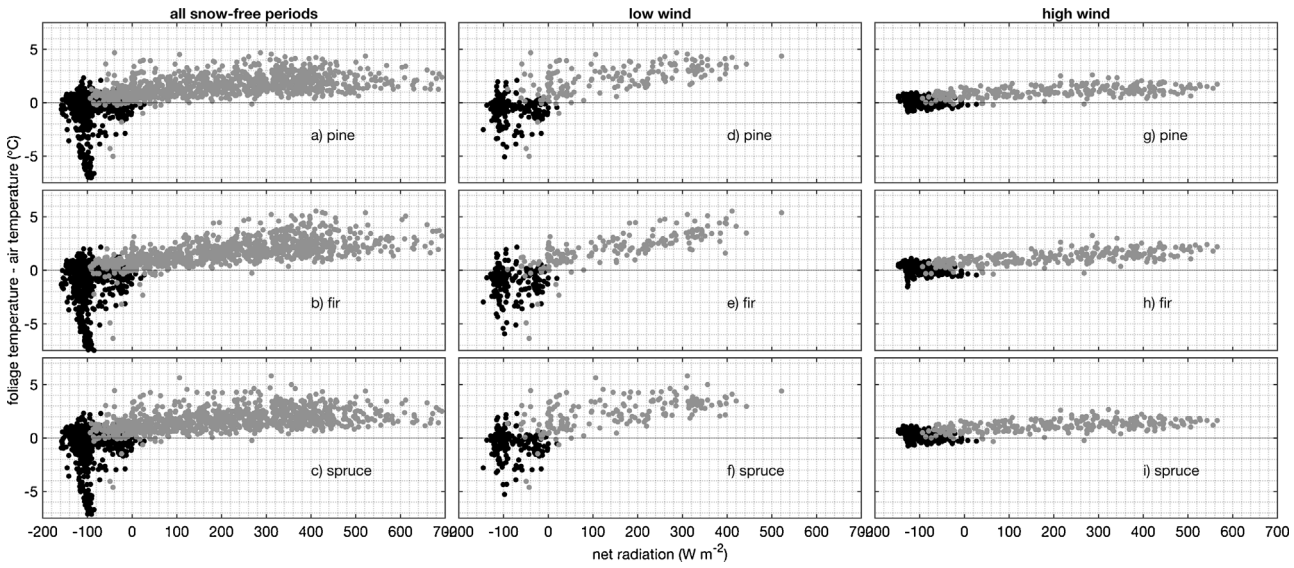

Fig. 2. Foliage temperature was measured using thermal infrared imaging. Periods with snow on the vegetation canopy were excluded. Day (gray) and night (black) are plotted separately, and data are plotted separately (in rows) for canopies of each tree species as indicated. The left column (a, b, c) includes all snow-free periods, the middle (d, e, f) and right (g, h, i) columns highlight those with low and high above-canopy horizontal wind velocity.

indicate exothermic and endothermic phase changes from liquid-ice and ice-liquid. These periods involved fairly constant bole temperature during the phase transitions (as one would observe in an ice bath). Data along the y-axis were grouped separately for each panel in Fig. 3 into 0.5 °C bins from −5 to 5 °C. Univariate frequency distributions were calculated, and the 98th percentiles are illustrated as circles in Fig. 3c. A regression through these data is shown (black line), and this regression line to the point where it intersected the origin on the x-axis was used as an indication of ice in the bole. All time periods left of the regression lines (or left of the origin at values below the y-intercepts, vertical black line) were considered to have frozen xylem in the boles.

Time series of air and bole temperature, sap flux voltage and density, and NEE during the winter-spring transition are shown in Fig. 4. No net carbon uptake was detected until the boles thawed in mid April (period 1). Boles were frozen prior to this (indicated by shading) for most of the winter. Air temperature during period 1 when the boles thawed was not substantially higher than in the previous month, although it was above freezing for a longer period (Fig. 4a). Radiative and

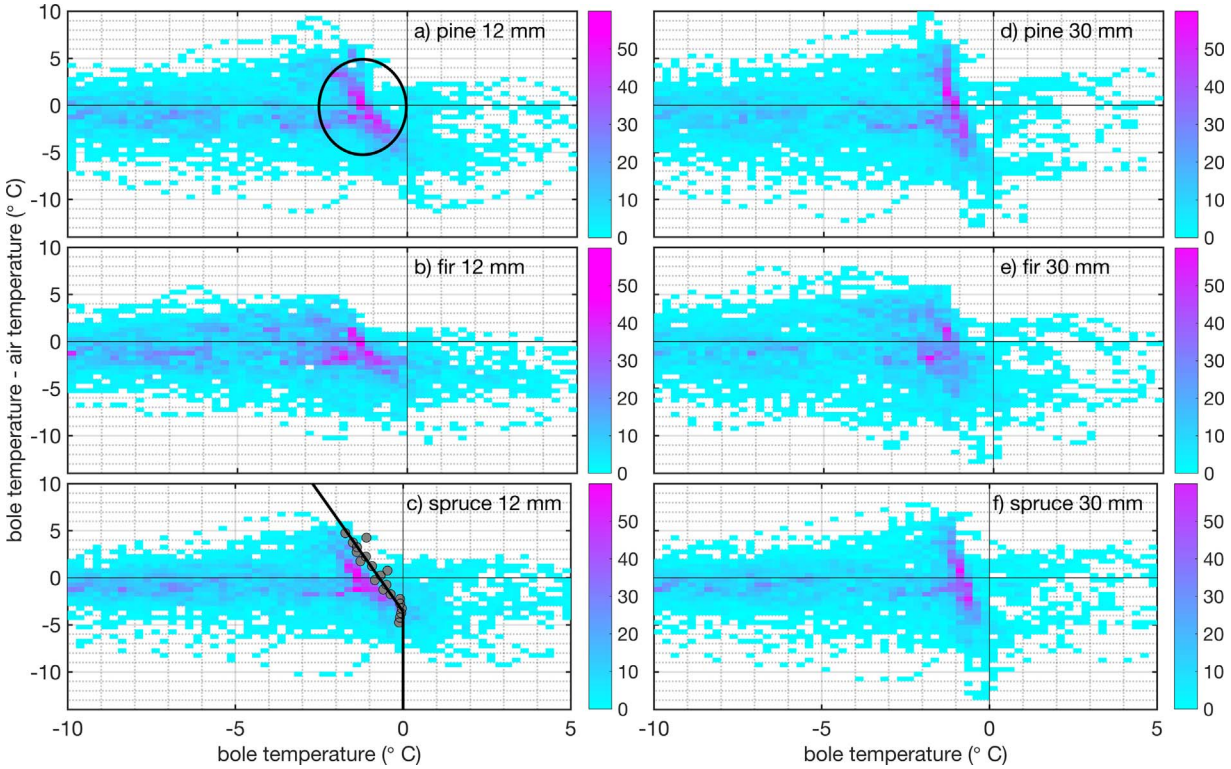

Fig. 3. The difference between bole temperature and air temperature (2m above ground) as a function of bole temperature during the period Nov 1–April 30. Data are plotted as bivariate frequency distributions, with the color bar indicating frequency of occurrence in each bin. Panels indicate different tree species (rows) and measurement depth within xylem (columns). The circle shown in a) indicates the general region of exothermic and endothermic phase changes, with high frequency over the cold season. Illustrated in c) is the method used to identify the presence of ice in the bole in each case (omitted on other panels for clarity, see text for details).

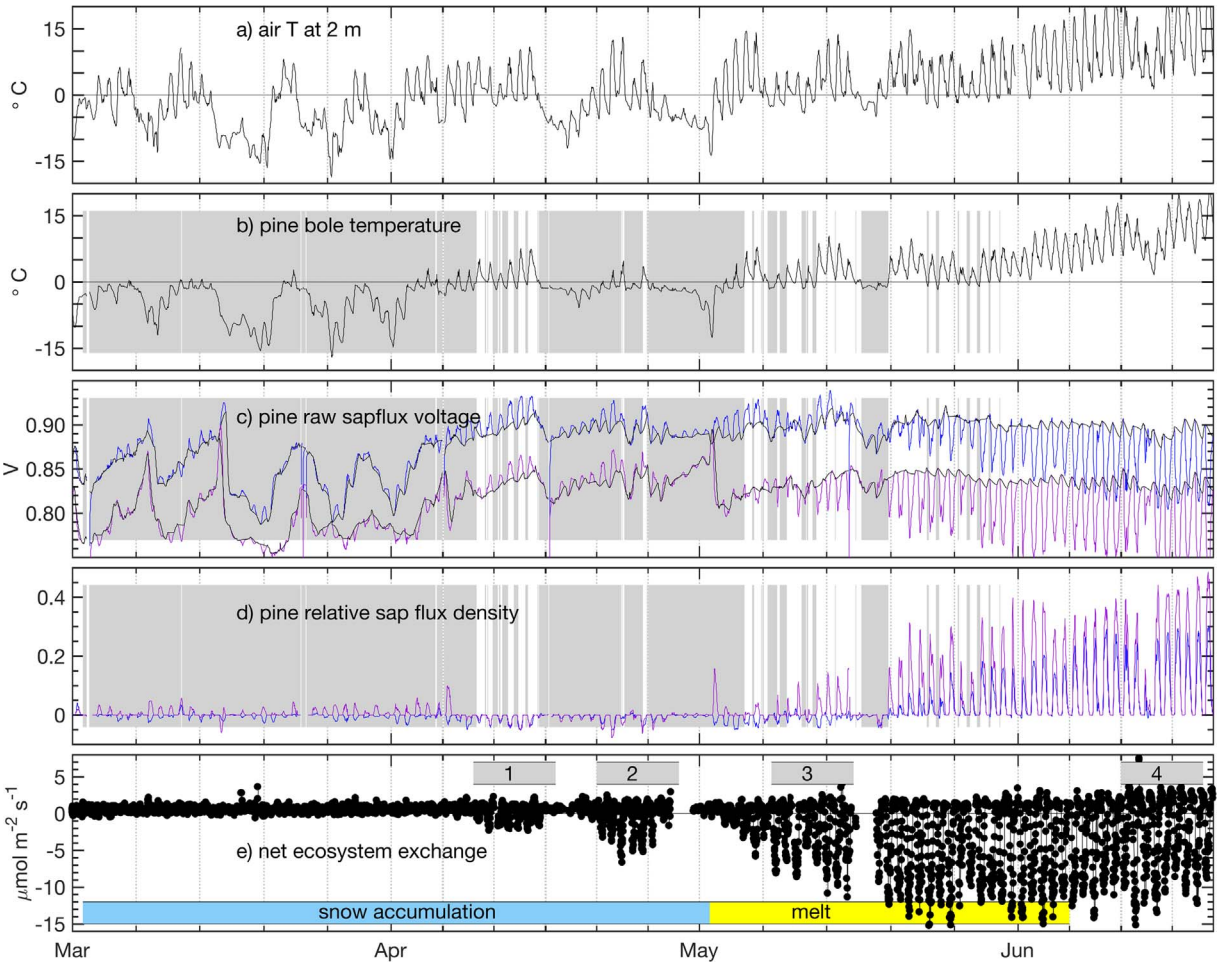

Fig. 4. Air (a) and bole (b) temperature compared to sapflux (c, d) and net ecosystem exchange of CO_2 (e) data during initiation of spring activity (March 1–June 20). Shaded boxes in the middle panels indicate periods with ice detected in the pine boles. Raw voltages (proportional to differential temperature) are shown in c) for the thermal dissipation sapflux sensor pairs in two pine trees (different colors) with the baseline voltages shown (black lines). These data were used to calculate relative sap flux density shown in d). Positive values in panel d) indicate water movement upward in the tree, but negative values do not indicate downward transport. Sap flux data were similar for spruce and fir and are omitted here for clarity. Net ecosystem exchange (e) is negative by our sign convention when the forest is a net sink for carbon. Boxes indicate the periods of snow accumulation and melt, and time periods of interest shown in Figs. 5 and 6, and S1. Thin white lines in the shading prior to period 1 are caused by a plotting software problem and don't indicate melt (see Fig. 6).

convective processes were likely also important for bole energy balance and associated thaw.

The raw voltage from sap flux sensor pairs was highly variable. Typical diel voltage patterns for TD sap flux sensors in warmer conditions are maximum at night and lower during the day when transpiration occurs, because they are proportional to the temperature difference between the sensors. The normal diel pattern was observed in late May and June (Fig. 4c), but large baseline shifts and unusual patterns of diel variability were apparent when boles were frozen (e.g., March, Fig. 4c) or thawing. When the boles thawed during period 1, the diel voltage pattern was maximum during the day and minimum at night (opposite the normal pattern). When sap flux density was calculated from these voltages (using the baselines shown in Fig. 4c), it was sometimes negative (period 1, Fig. 4d). The TD technique cannot distinguish direction of flow, so the negative value is an artifact of the thawing process, but illustrates that normal bole sap transport was not observed in the region of the sap flux sensors during this time. There was no clear difference between plant species in the timing of initiation of sap flux.

The spring initiation of sap flux transport was delayed relative to NEE (Fig. 4d,e). Time periods were selected for closer examination based on NEE data to evaluate initiation of photosynthesis (period 1), and the multi-week transition (periods 2 and 3) to maximum photosynthesis (period 4). Net ecosystem exchange indicated net carbon uptake during the spring transition when boles were thawed (periods 1, 3, and 4), but also during an intermittent period with warm air and frozen boles (period 2). Sustained cold periods between periods 1–3 involved ice in boles and decrease or absence of net carbon gain (note that some NEE data are missing). Considerable spatial variation probably exists in the ice-liquid state within the trees; detection of ice at a few bole locations may or may not be representative of the tree (or forest) as a whole.

The responses of sap flux density and NEE to PAR are shown for periods 1–4 in Fig. 5. Regions where fitted curves do not overlap indicate statistically significant differences; no difference in the light response of sap flux density was detected during periods 1 and 2 (Fig. 5a), but other periods were statistically different for all the fluxes. Appreciable sap flux transport did not occur until period 3, but NEE showed a clear dependence on light during all these periods. The light dependence of both NEE and GPP increased continually from period 1 to period 4 (Fig. 5b,c). The canopy-level photosynthetic capacity (GPP_{sat}, intersection of each fitted line in Fig. 5c with vertical line) increased 5-fold (2.2 to 11.6 μmol m^{-2} s^{-1}) between periods 1 and 4. This pattern of gradual yet continual increase in activity over time was consistent when the flux partitioning was done with soil temperature (Fig. 5) or with air temperature (Supplemental Fig. S1), although the magnitudes of GPP and R_{eco} differed based on the temperature choice. These changes in the magnitudes of sap flux density and NEE occurred during

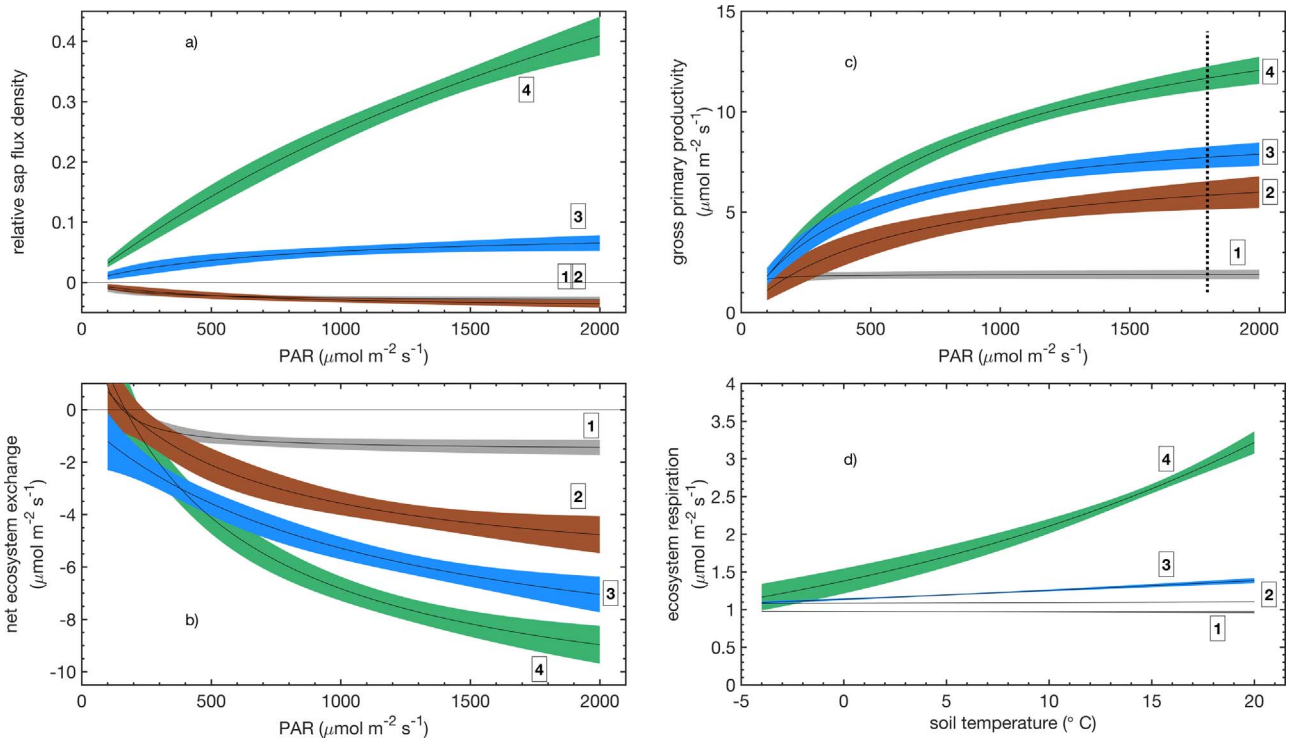

Fig. 5. The light responses of transpiration (a, relative sap flux density) and net ecosystem exchange (b) in the daytime, during the four periods indicated in Fig. 4. Shown are curve fits (solid lines) with shading indicating 95% confidence bounds - some periods overlap (e.g., periods 1 and 2 in (a)). Color shading is consistent between panels. Plotted in c) and d) are the light response of GPP and temperature response of ecosystem respiration, respectively, during the four periods. The canopy-level photosynthetic capacity index (GPP_{sat}, shown in Fig. 7b) for each period is illustrated by the intersection of each fit with the vertical line at 1800 μmol m^{-2} s^{-1} in c). The fluxes were partitioned using the method of Reichstein et al. (2005) using soil temperature (or air temperature for comparison in Supplemental Fig. S1). Vegetation and air temperature during these periods are provided in Table 2. Periods with ice in the boles were excluded.

Table 3
Temperature (°C) of tree crowns (mean of 6 individual crowns, 2 per species) measured via thermal imagery, and air (21 m height, thermistor) during the four periods of interest shown in Figs. 4–6 and Supplemental Fig. S1. Data shown are mean and standard deviation of daytime periods when the foliage was snow-free (n = number of half-hour periods).

time period	crown temperature		air temperature	
	mean (SD) (°C)	n	mean (SD) (°C)	n
1: April 9–17	no data	no data	4.2 (3.9)	110
2: April 21–29	8.4 (3.4)	21	6.9 (3.5)	29
3: May 8–16	7.9 (4.3)	118	5.0 (3.5)	152
4: June 11–19	16.8 (4.5)	197	14.1 (3.5)	210

concomitant increases in air and foliage temperature (Table 3), particularly so during period 4 in June.

The seasonal patterns of sap flux density and NEE during autumn, winter, and spring are compared to bole temperature and needle pigments in Fig. 6. For most of the winter when the boles were frozen, NEE was small and positive due to R_{eco}, and sap transport (and thus transpiration) did not occur. Seasonality of pigment composition (or the lack of it) was qualitatively consistent across plant species (Figs. 6 and 7, S2). The total chlorophyll content of needles varied among species, with higher content in fir needles than pine or spruce (Fig. 6). There were no seasonal changes in total chlorophyll (Fig. 6a), lutein, or β-carotene content, or in the chlorophyll *a/b* ratio (Fig. S2). The overall xanthophyll cycle pool size was highest in mid-winter and lowest in summer (Fig. S2). The deepoxidation state of the xanthophyll cycle ([A + Z]/[V + A + Z], Fig. 6b) exhibited a marked seasonal shift to a constant winter state that was co-incident with lack of transpiration and photosynthesis in winter (Fig. 6d,e) and presence of ice in the boles (Fig. 6c). There was variability in the xanthophyll cycle deepoxidation state among species during the fall and winter transitions (Fig. 6b).

The seasonal pattern of xanthophyll cycle deepoxidation state (Fig. 7a) was similar to the seasonal pattern of GPP and GPP_{sat} (Fig. 7b); the deepoxidation state began to fall from mid-winter peak values just as appreciable GPP was observed. However, the maximum GPP was reached in late May, and the deepoxidation state continued to fall for a couple of weeks thereafter. The linear relations between deepoxidation state and GPP_{sat} were statistically significant (Fig. 8a) but with low r^2 due to the difference in timing.

The ratio of chlorophyll to carotenoid pigments varied across the season in a sinusoidal-like fashion, highest in summer and lowest in winter, and was qualitatively similar among species (Fig. 7c). This pattern was similar to the seasonality of solar forcing (solar elevation angle) and the indices of G_{CC} and GRVI (Fig. 7d), but with phase differences. The latter were delayed in their spring increase relative to the solar forcing, with GRVI increasing latest. The spring increase in canopy-level photosynthetic capacity (Fig. 7b) was 4–6 weeks after the spring equinox. Despite the phase differences between the two indices, G_{CC} and GRVI were both strongly and significantly correlated with GPP_{sat} on a 10-day basis (Fig. 8b, c), with higher r^2 for the G_{CC} versus GPP_{sat} relation.

4. Discussion

4.1. Temperature limitation to photosynthesis

Our primary objective was to test the hypothesis that climate has warmed sufficiently to allow this high-elevation forest to photosynthesize during favorable warm periods in winter. Despite many warm, sunny days with leaf temperature favorable for photosynthesis, the forest remained dormant from late October through early April, with no appreciable GPP observed. After recovery from winter

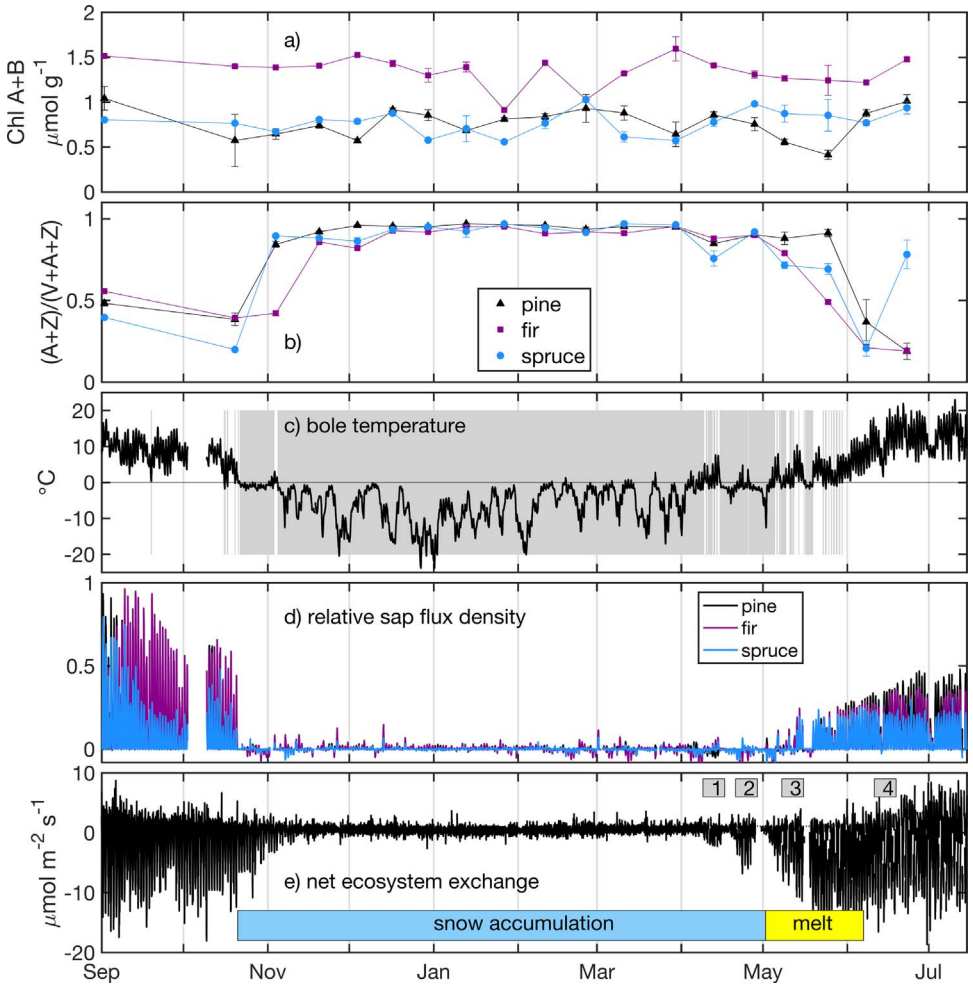

Fig. 6. The seasonal patterns of a) concentration of total leaf chlorophyll for each species (means and standard deviations shown), b) midday deepoxidation state of leaf xanthophyll pigments for each species, c) bole temperature (pine, 12 mm depth in xylem) with frozen xylem indicated by gray shading, d) transpiration (relative sap flux density, colors indicate means for different species), and e) net ecosystem exchange. The difference in magnitude of transpiration before and after winter is probably meaningless since the sensors were not replaced. Boxes indicate the periods of snow accumulation and melt, and time periods of interest in Figs. 4 and 5, and S1.

downregulation, the temperature optimum for early-season branch-level photosynthesis of these species is ~10 °C, and photosynthesis rates at 5 °C are nearly as high (Huxman et al., 2003). Whole-forest carbon gain is optimal in the range 10–15 °C across the full growing season (Huxman et al., 2003). During the cold season in our study, foliage temperature reached 5 °C in all months, and occasionally above 10 °C (Table 2). Temperature of individual crowns during the cold season was similar between species (Supplemental Table S1), in contrast with findings from summer showing consistent species differences (Aubrecht et al., 2016; Leuzinger and Körner, 2007). Despite the warm days, after dormancy began in fall, no net carbon exchange or sap transport was observed until April (Figs. 4 and 6). Hence winter photosynthesis was limited by more than just the direct effect of leaf temperature on metabolism.

4.2. Water limitation to photosynthesis

The hydraulic continuum from soil to atmosphere was blocked by ice in the boles, preventing water transport for much of the winter (Fig. 6). Frozen xylem sap was easily identified by comparing bole and air temperature (Fig. 3). Bole temperature in winter is rarely reported, but the phase changes apparent in Fig. 3 are similar to those studies available (Hadley, 2000; Mayr et al., 2006). Sparks et al. (2001) showed that the ice fraction of frozen lodgepole pine boles under similar ambient temperature was maximally 75%, so some liquid water was probably always present in the boles. Gutmann et al. (2017) have shown that trees at this forest compress and expand longitudinally, as ice formation responds to air temperature variation in the range −3–−20 °C, further evidence of the variable nature of bole freezing.

We did not measure the temperature of distal small twigs, but given the high daily variability of foliage temperature (Fig. 1, Table 2), twigs likely experienced well over 100 freeze-thaw cycles (FTCs) during the winter. Frozen xylem with warm foliage probably led to large time-varying gradients of water potential in distal twigs (Mayr and Charra-Vaskou, 2007) caused by very low water potential in twigs during thaw (Mayr et al., 2003). Recurring FTCs can lead to progressive reduction in hydraulic conductivity of xylem as tracheids become embolized, and up to 30% loss of conductivity in winter has been observed in these species (Sparks et al., 2001; Sperry et al., 1994). Conifers generally refill embolized tracheids at end of winter (Sperry et al., 1994); mechanisms for this remain unclear (Zwieniecki and Holbrook, 2009) but direct leaf uptake of melting snow in the canopy has been suggested (Mayr et al., 2014; Sparks et al., 2001). Hence there were limitations to plant water transport by ice and xylem embolism during most of the cold season.

There was little evidence, however, to suggest that frozen soil water limited sap transport. Soil temperature at multiple depths was nearly always above the freezing point for pure water, and with the influence of solutes, soils remain unfrozen well below 0 °C (Edwards and Cresser, 1992). No indication of freezing was apparent in the soil moisture data (Fig. 1a) as is common with water content reflectometers (e.g., Bowling et al., 2010). Fall soil moisture persisted with only minor change through most of the winter until the first melt events in April (Fig. 1), providing further evidence for no transpiration during winter. Persistent soil moisture from late autumn into midwinter, and relatively warm soils under the snowpack are common for temperate mid-latitude forests of the western United States (Maurer and Bowling, 2014). Monson et al. (2005) identified isothermality of the snowpack and related melt infiltration into the soil as a key event for initiating

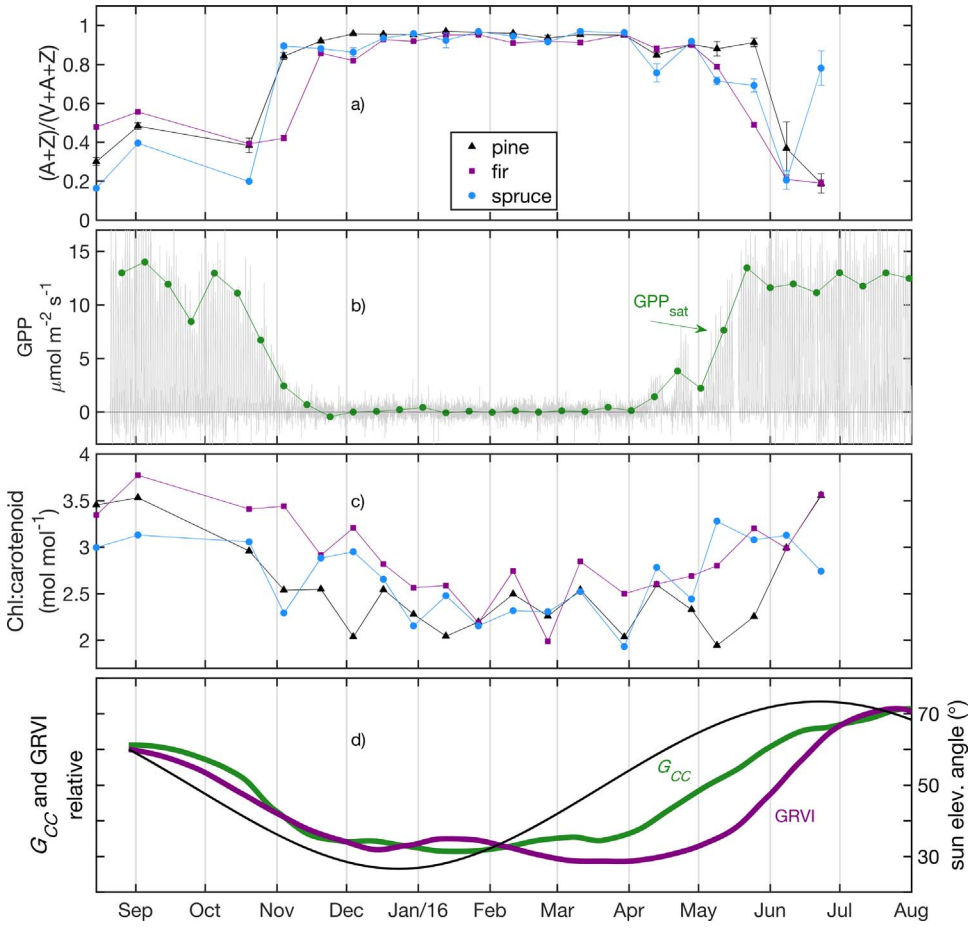

Fig. 7. The seasonal patterns of a) midday deepoxidation state of leaf xanthophyll pigments for each species (as in Fig. 6b) hourly daytime gross primary productivity (gray shading) and 10-day mean canopy-level photosynthetic capacity index (GPP_{sat}, green) as illustrated in Fig. 5c) the ratio of total chlorophyll to total carotenoid pigments in leaves of each species, and d) the midday Green Chromatic Coordinate (G_{cc}, green) and Green-Red Vegetation Index (GRVI, purple) calculated from visible imagery, and solar elevation angle (thin black line).

photosynthesis of this forest in spring. Our results do not necessarily contradict this, since the boles thawed (Fig. 4b) concomitantly with the first soil moisture increase (Fig. 1a) in mid-April, but prolonged ice in the boles appears to have been the primary limitation to water transport. Soil moisture did not increase by much until late May, well into the snowmelt period (Fig. 1) and ~6–7 weeks after net carbon uptake was first detected (Fig. 4). We note, however, that cold (< 5 °C) soil dramatically reduces root hydraulic conductivity, limiting both photosynthesis and stomatal conductance in these species even when water is plentiful (Day et al., 1989; DeLucia, 1986; Kaufmann, 1975; Running and Reid, 1980). The role of cold soils in limiting photosynthesis may be particularly important during the spring recovery period (Ensminger et al., 2008).

4.3. Spring initiation of carbon uptake and water transport

Net carbon uptake did not begin until boles thawed in period 1 (Figs. 4 and 6). We anticipated that water transport in boles would precede initiation of photosynthesis, and thus sap transport would be detected before net carbon gain was observed via eddy covariance, but this did not occur (periods 1 and 2, Fig. 4). These data strongly suggest water transport in the boles was blocked by frozen xylem, preventing water uptake from soil, and potentially contributing to the inhibition of photosynthesis on warm winter days. When branches of these species were collected in winter and allowed to return to function under favorable laboratory conditions, there were species differences in recovery rates of photosynthesis (Monson et al., 2005). There was no difference, however, between species in the timing of bole thaw (data not shown), or in initiation of sap transport (Fig. 6). Without branch-level gas exchange data, we cannot determine if the three species initiated photosynthesis at different times, but their sap transport timing did not differ.

Net carbon uptake began (period 1) as diel variation in raw sap flux voltage was detected when the boles first thawed (Fig. 4), but as noted the diel variation was opposite the normal pattern, indicating that normal sap transport did not occur. The light responses of both NEE and GPP increased more rapidly than sap transport over the ensuing several weeks (Fig. 5), which serves as evidence for decoupling of carbon and water fluxes at the scale of individual trees. During periods 1 and 2, photosynthesis occurred even though there was no sap transport detected (Fig. 5). In fact, the boles were frozen during much of period 2 (Fig. 4). If these sap flux data are correct, this indicates that sufficient stored water to support cellular metabolism was present as photosynthetic activity ramped up while evaporative demand (vapor pressure deficit, VPD) remained low. Sevanto et al. (2006) found that in Scots pine in southern Finland, spring photosynthesis began 2–7 days before diel stem diameter variation occurred, evidence that trees initially relied on stored stem water for photosynthesis before transporting water from the soil.

Peak summer daily water use of the trees at the Niwot forest in is roughly 10, 5, and 3 L H_2O $tree^{-1}$ d^{-1}, for pine, spruce, and fir, respectively, and transpiration of these species is highly dependent on humidity (Hu et al., 2010; Pataki et al., 2000). Evaporative demand was low during periods 1 and 2 (maximum VPD was 0.65 and 0.58 kPa, respectively), so total water demand for transpiration would likely be several-fold less than the summer peak values. Sapwood volume for these species in similar size class (12–50 cm DBH) at the Fraser Experimental Forest (30 km distant and similar elevation), was determined allometrically at 31 ± 41, 37 ± 55, and 12 ± 17 L $tree^{-1}$ (mean ± SD) for pine, spruce, and fir, respectively (Ryan, 1989). Thus it seems reasonable that the volume of stored water in the trees would be sufficient to support initial C uptake at end of winter, even if some of

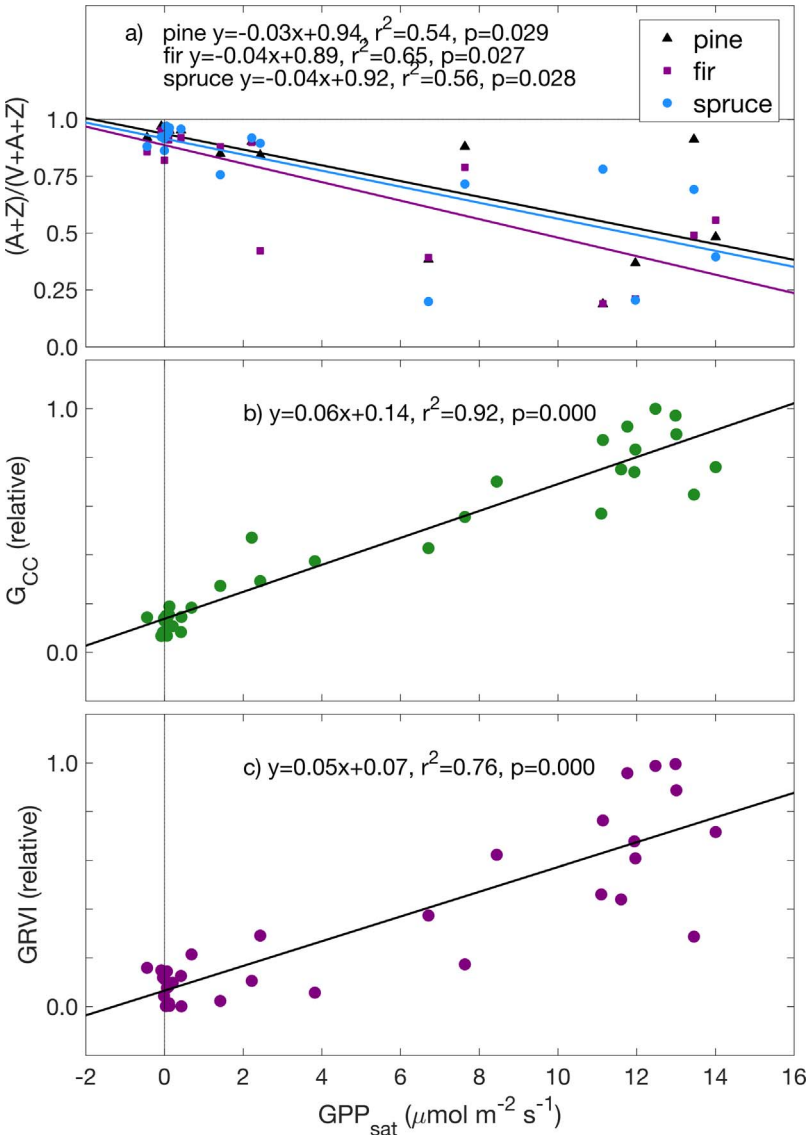

Fig. 8. Comparisons of a) midday deepoxidation state of leaf xanthophyll pigments for each species, b) the G_{CC} and c) GRVI indices with GPP_{sat}, for 10-day periods shown in Fig. 7b. Linear regression parameters are shown for each, with p-values indicating significance of the regression slope (t-test).

that water were frozen.

It remains possible that frozen boles did not fully block sap transport. None was detected at our probe depth (21 mm) when boles were frozen (Figs. 4 and 6), but we cannot rule out the possibility of sap transport closer to the center of the bole. Summer sap velocity of these species does vary radially, with peak velocity 20–40 mm into the xylem (Mark and Crews, 1973). We note that in our study the sap flux observations were required to compare relative timing of photosynthesis and water transport during the winter-spring transition. Eddy-covariance-based comparisons of NEE and water vapor flux were not useful due to high latent heat flux from snow sublimation in the cold season (Molotch et al., 2007). More work with alternate sap flux techniques (Vandegehuchte and Steppe, 2013) would be useful to further elucidate the importance of winter ice blockage of sap transport.

4.4. Biochemical limitation to photosynthesis

Our data indicate a significant role for the xanthophyll cycle pigments in winter downregulation and photoprotection. (Fig. 6). The winter increase in xanthophyll cycle pool size is often accompanied by seasonal decrease in total chlorophyll content (Ensminger et al., 2004; Porcar-Castell et al., 2012; Wong and Gamon, 2015a), and a seasonal increase in lutein content (Verhoeven, 2014), but in our study trees neither total chlorophyll nor lutein varied seasonally (Fig. 6a and S2). We did not detect photosynthesis during almost all of the time the xanthophyll cycle was in the highly photoprotective state (Fig. 6b,e), even during warm sunny days (Fig. 1d). This is consistent with the slowly-reversible form of energy dissipation serving as a sustained form of photoprotection during the winter (Verhoeven, 2014). Note, however, that during the fall and spring transition seasons, the xanthophyll cycle was sometimes in the highly photoprotective state during periods of carbon gain (including periods 1–3, Fig. 6b, e). This could be due to the additional presence of the rapidly-reversible form of photoprotection at these times, as we did not sample the needles in the dark. We cannot distinguish between the two forms without additional measurements (e.g., chlorophyll fluorescence or leaf gas exchange, or leaf spectral reflectance - see PRI below).

Gross primary productivity took 5–6 weeks to reach maximum summer levels, coinciding with the first appearance of xanthophyll cycle deepoxidation states below mid-winter peak values. Monson et al. (2005) suggested that physiological recovery from winter dormancy in this forest is 1) initiated by response to warm air temperature and recovery of photosystem II function, leading to disengagement of sustained photoprotective thermal energy dissipation, 2) continued as the hydraulic system recovers, and 3) completed as the carboxylation reactions fully recover. Comparison of timing of bole thaw, initiation of

sap transport, and initiation of photosynthesis (Figs. 4 and 6) indicates that hydraulic system recovery may actually be important during the earliest stages of recovery. The xanthophyll cycle remained largely in the deepoxidized (photoprotective) state for several weeks after initiation of photosynthesis. However, one should note that our measures of relaxed xanthophyll cycle deexpoxidation states during the spring transition are conservative because we were unable to control for the time of day of pigment sampling (that is, we cannot be certain that predawn xanthophyll cycle deepoxidation states would not have relaxed somewhat sooner in the spring).

4.5. Implications for modeling

There is a growing appreciation within soil-plant-atmosphere, ecosystem, and land surface models for the need to incorporate whole-plant hydraulic processes, and variability in hydraulic traits, to better understand coupled carbon and water cycling (Bonan et al., 2014; Matheny et al., 2017; Sperry et al., 2016). These efforts are mainly focused on improving model representation of plant response to drought (e.g., Christoffersen et al., 2016; Xu et al., 2016). To our knowledge, none of these models incorporate mechanistic details of seasonal downregulation of photosynthesis, certainly not via photoprotection or ice blockage of xylem. For example, in CLM 4.5, the temperature response of photosynthesis is derived from the Farquhar et al. (1980) photosynthesis model, and applies an exponential function to adjust photosynthetic capacity as a function of temperature (Oleson et al., 2013). Mathematically this formulation reduces but does not eliminate photosynthesis at subzero temperature. Additional factors based on soil moisture, influenced by the fraction of frozen soil, and day length lead to further reductions in modeled photosynthesis during the cold season. However, without site-specific calibration, CLM 4.5 erroneously predicts GPP year-round at Niwot Ridge (Raczka et al., 2016). Because seasonal snow cover affects ecosystems covering half the Northern Hemisphere land surface (Zhang et al., 2004), improvements in process modeling of photosynthesis and its downregulation in cold conditions are warranted.

4.6. Visible imagery and seasonality of GPP

Our secondary objective was to determine if visible-wavelength imagery could be used to identify periods of activity and dormancy. Examination of NEE and water fluxes across climate or elevation gradients (Anderson-Teixeira et al., 2010; Goulden et al., 2012; Liu et al., 2016) has been useful to understand seasonality of GPP, but results from flux studies like these could be greatly expanded if linked to digital camera imagery or remote sensing to quantify the effects of climate and climate change on evergreen seasonality and productivity across the landscape. Indices derived from repeat photography with digital cameras such as the G_{CC} or GRVI are closely related to GPP in deciduous forests (Keenan et al., 2014; Motohka et al., 2010; Wingate et al., 2015). In evergreen forests, however, the amount of light absorbed and the light use efficiency of photosynthesis vary seasonally (as we have shown here). For this reason, visible camera imagery and satellite derived visible-wavelength vegetation indices have not been particularly useful for determining seasonality of productivity of evergreen forests (e.g., Garbulsky et al., 2008; Wingate et al., 2015). Here, even though the G_{CC} and GRVI were modestly out of phase relative to GPP_{sat} (Fig. 7b,d), both indices were strongly correlated with GPP_{sat} (Fig. 8).

A recent study highlighted a new remotely-sensed pigment index that tracks the temporal change in evergreen photosynthesis at several spatial scales (Gamon et al., 2016). Studies with lodgepole pine seedlings showed that initiation of photosynthesis in spring was related to the ratio of chlorophyll to carotenoid pigments, and also to the deepoxidation state of xanthophyll pigments (Wong and Gamon, 2015a, 2015b). Based on these results, Gamon and colleagues developed a new MODIS-based algorithm called the CCI (chlorophyll/carotenoid index) that was an effective predictor of seasonality of GPP in 3 conifer forests of North America. Data from the MODIS bands required for this were not yet widely available at the time of our analysis, but they are red (620–670 nm) and green (526-536 nm) reflectance bands, and the CCI is thus similar to the GRVI (Motohka et al., 2010; Tucker, 1979). In our case, both G_{CC} and GRVI (calculated from visible imagery and thus similar in concept to CCI) were robust estimators of GPP_{sat} (Fig. 8). Note that these indices highlight seasonality of canopy color that occurs without change in total chlorophyll (Fig. 6 a) or in relative amounts of chlorophyll A and B (Figure S2a), implying that the carotenoids, particularly the xanthophyll cycle pigments (Figure S2b), are important for the color change. The spectral response of our PhenoCam has a green peak at ~530 nm, which is similar to the 531 nm band used in the photochemical (or physiological) reflectance index (PRI, Wong and Gamon, 2015a) which tracks xanthophyll cycle deepoxidation state, and also similar to MODIS band 11 used in the CCI (Gamon et al., 2016). This adds to the building evidence that simple metrics like the G_{CC}, GRVI, CCI, or PRI, may indeed be useful for assessing seasonality of GPP in conifer forests. We note that careful calibration and consistent protocols are required (Balzarolo et al., 2011; Gamon et al., 2010; Sonnentag et al., 2012).

The timing of the spring transitions for G_{CC} and GRVI were a bit different than GPP_{sat}, contrasting with the results of Gamon et al. (2016). This could be due to the spectral differences in our measured GRVI and CCI, lack of seasonality of chlorophyll content (Fig. 6a), or different pigment-dependent photoprotection strategies such as the relative degree of rapidly reversible energy dissipation (Verhoeven, 2014), the lutein epoxide cycle (Jahns and Holzwarth, 2012), or zeaxanthin-independent processes related to photosynthetic downregulation (Fréchette et al., 2015). Note that we did not find a strong correspondence of seasonal pattern between the measured chlorophyll to carotenoid ratio (Fig. 7c) and GPP (Fig. 7b) as reported by Wong and Gamon (2015a). Studies are needed that continue to examine reflectance indices like G_{CC}, GRVI, CCI, and PRI, and other promising indices such as solar-induced fluorescence (Jeong et al., 2017; Porcar-Castell et al., 2014; Walther et al., 2016) in the context of evergreen GPP at scales from chloroplast to flux tower to satellite remote sensing.

5. Conclusions

We evaluated the hypothesis that climate has warmed sufficiently to allow the high-elevation subalpine conifers at Niwot Ridge to photosynthesize during favorable warm periods in winter. Despite many warm, sunny days with leaf temperature favorable for photosynthesis, no carbon gain was detected in this forest from late October through early April. Temperature was not a direct metabolic limitation to photosynthesis, but frozen boles provided a direct limitation to water transport, and only as the boles thawed did photosynthesis return in the spring. The snowpack kept soils warm enough so that frozen soil was not a limitation to water transport. Spring initiation of photosynthesis occurred prior to detection of sap transport in boles, indicating the importance of stored water in the bole or uptake of melt water by the foliage. Seasonal biochemical adjustments included an increase in xanthophyll cycle pool size relative to chlorophyll, and sustained conversion of violaxanthin to antheraxanthin and zeaxanthin, but minimal seasonal change in chlorophyll content or that of other carotenoids. Associated changes in leaf color were observed in visible-band digital camera imagery, suggesting the potential for broad-scale monitoring of the seasonality of evergreen photosynthetic potential using airborne or near-surface remote sensing.

Acknowledgements

Many thanks to Dave Hollinger, Bev Law, and the AmeriFlux Management Project team for their leadership of the AmeriFlux

community over the last 20 years. We are grateful to John Gamon and Brett Raczka for helpful discussions, for assistance in the field to Brett Boyer, Hilary Buchanan, and Jen Morse, to Brent Helliker for sharing equipment, and to Jia Hu, Dave Moore, Diane Pataki, and the USDA/NRCS Snow Survey Program for sharing data. This research was primarily supported by the U.S. Department of Energy, Office of Science, Office of Biological and Environmental Research, Terrestrial Ecosystem Science Program under Award Number DE-SC0010625. Additional funding was provided by National Science Foundation (NSF) EPSCoR grant IIA 1208732 awarded to Utah State University, as part of the State of Utah Research Infrastructure Improvement Award. ADR acknowledges support from the NSF Macrosystems Biology program (grant numbers EF-1241616, EF-1065029). The US-NR1 site is currently supported by the U.S. Department of Energy, Office of Science, through the AmeriFlux Management Project (AMP) at Lawrence Berkeley National Laboratory under award number 7094866.

Appendix A. Supplementary data

Supplementary material related to this article can be found, in the online version, at doi:https://doi.org/10.1016/j.agrformet.2018.01.025.

References

Adams, W.W., Demmig-Adams, B., 1992. Operation of the xanthophyll cycle in higher plants in response to diurnal changes in incident sunlight. Planta 186, 390–398. http://dx.doi.org/10.1007/BF00195320.

Adams, W.W., Zarter, C.R., Ebbert, V., Demmig-Adams, B., 2004. Photoprotective strategies of overwintering evergreens. BioScience 54, 41–49. http://dx.doi.org/10.1641/0006-3568(2004)054[0041:PSOOE]2.0.CO;2.

Anderson-Teixeira, K.J., Delong, J.P., Fox, A.M., Brese, D.A., Litvak, M.E., 2010. Differential responses of production and respiration to temperature and moisture drive the carbon balance across a climatic gradient in New Mexico. Global Change Biol. 17, 410–424.

Aubrecht, D.M., Helliker, B.R., Goulden, M.L., Roberts, D.A., Still, C.J., Richardson, A.D., 2016. Continuous, long-term, high-frequency thermal imaging of vegetation: uncertainties and recommended best practices. Agric. For. Meteorol. 228–229, 315–326. http://dx.doi.org/10.1016/j.agrformet.2016.07.017.

Balzarolo, M., Anderson, K., Nichol, C., Rossini, M., Vescovo, L., Arriga, N., Wohlfahrt, G., Calvet, J.-C., Carrara, A., Cerasoli, S., Cogliati, S., Daumard, F., Eklundh, L., Elbers, J.A., Evrendilek, F., Handcock, R.N., Kaduk, J., Klumpp, K., Longdoz, B., Matteucci, G., Meroni, M., Montagnani, L., Ourcival, J.-M., Sánchez-Cañete, E.P., Pontailler, J.-Y., Juszczak, R., Scholes, B., Martín, M.P., 2011. Ground-based optical measurements at European flux sites: a review of methods, Instruments and current controversies. Sensors 11, 7954–7981. http://dx.doi.org/10.3390/s110807954.

Barichivich, J., Briffa, K.R., Myneni, R.B., Osborn, T.J., Melvin, T.M., Ciais, P., Piao, S., Tucker, C., 2013. Large-scale variations in the vegetation growing season and annual cycle of atmospheric CO2 at high northern latitudes from 1950 to 2011. Global Change Biol. 19, 3167–3183. http://dx.doi.org/10.1111/gcb.12283.

Bonan, G.B., Williams, M., Fisher, R.A., Oleson, K.W., 2014. Modeling stomatal conductance in the earth system: linking leaf water-use efficiency and water transport along the soil–plant–atmosphere continuum. Geosci. Model Dev. 7, 2193–2222. http://dx.doi.org/10.5194/gmd-7-2193-2014.

Bowling, D.R., Bethers-Marchetti, S., Lunch, C.K., Grote, E.E., Belnap, J., 2010. Carbon, water, and energy fluxes in a semiarid cold desert grassland during and following multiyear drought. J. Geophys. Res. G: Biogeosci. 115.

Brooks, P.D., Grogan, P., Templer, P.H., Groffman, P., Öquist, M.G., Schimel, J., 2011. Carbon and nitrogen cycling in snow-covered environments. Geogr. Compass 5, 682–699.

Brown, R.D., Mote, P.W., 2009. The response of Northern Hemisphere snow cover to a changing climate. J. Clim. 22, 2124–2145.

Burns, S.P., Blanken, P.D., Turnipseed, A.A., Hu, J., Monson, R.K., 2015. The influence of warm-season precipitation on the diel cycle of the surface energy balance and carbon dioxide at a Colorado subalpine forest site. Biogeosciences 12, 7349–7377. http://dx.doi.org/10.5194/bg-12-7349-2015.

Campbell, G.S., Norman, J.M., 1998. An Introduction to Environmental Biophysics. Springer.

Chan, A.M., Bowling, D.R., 2017. Assessing the thermal dissipation sap flux density method for monitoring cold season water transport in seasonally snow-covered forests. Tree Physiol. 37, 984–995. http://dx.doi.org/10.1093/treephys/tpx049.

Christoffersen, B.O., Gloor, M., Fauset, S., Fyllas, N.M., Galbraith, D.R., Baker, T.R., Kruijt, B., Rowland, L., Fisher, R.A., Binks, O.J., Sevanto, S., Xu, C., Jansen, S., Choat, B., Mencuccini, M., McDowell, N.G., Meir, P., 2016. Linking hydraulic traits to tropical forest function in a size-structured and trait-driven model (TFS v.1-Hydro). Geosci. Model Dev. 9, 4227–4255. http://dx.doi.org/10.5194/gmd-9-4227-2016.

Clow, D.W., 2010. Changes in the timing of snowmelt and streamflow in Colorado: A response to recent warming. J. Clim. 23, 2293–2306.

Day, T.A., DeLucia, E.H., Smith, W.K., 1989. Influence of cold soil and snowcover on photosynthesis and leaf conductance in two Rocky Mountain conifers. Oecologia 80, 546–552.

DeLucia, E.H., 1986. Effect of low root temperature on net photosynthesis, stomatal conductance and carbohydrate concentration in Engelmann spruce (Picea engelmannii Parry ex Engelm.) seedlings. Tree Physiol. 2, 143–154.

Edwards, A.C., Cresser, M.S., 1992. Freezing and its effect on chemical and biological properties of soil. Adv. Soil Sci. 18, 59–79.

Ensminger, I., Schmidt, L., Lloyd, J., 2008. Soil temperature and intermittent frost modulate the rate of recovery of photosynthesis in Scots pine under simulated spring conditions. New Phytol. 177, 428–442. http://dx.doi.org/10.1111/j.1469-8137.2007.02273.x.

Ensminger, I., Sveshnikov, D., Campbell, D.A., Funk, C., Jansson, S., Lloyd, J., Shibistova, O., Öquist, G., 2004. Intermittent low temperatures constrain spring recovery of photosynthesis in boreal Scots pine forests. Global Change Biol. 10, 995–1008. http://dx.doi.org/10.1111/j.1365-2486.2004.00781.x.

Farquhar, G.D., von Caemmerer, S., Berry, J.A., 1980. A biochemical model of photosynthetic CO2 assimilation in leaves of C3 species. Planta 149, 78–90.

Forkel, M., Carvalhais, N., Rödenbeck, C., Keeling, R., Heimann, M., Thonicke, K., Zaehle, S., Reichstein, M., 2016. Enhanced seasonal CO2 exchange caused by amplified plant productivity in northern ecosystems. Science 351, 696–699. http://dx.doi.org/10.1126/science.aac4971.

Fréchette, E., Wong, C.Y.S., Junker, L.V., Chang, C.Y.-Y., Ensminger, I., 2015. Zeaxanthin-independent energy quenching and alternative electron sinks cause a decoupling of the relationship between the photochemical reflectance index (PRI) and photosynthesis in an evergreen conifer during spring. J. Exp. Bot. (66), 7309–7323. http://dx.doi.org/10.1093/jxb/erv427.

Gamon, J.A., Coburn, C., Flanagan, L.B., Huemmrich, K.F., Kiddle, C., Sanchez-Azofeifa, G.A., Thayer, D.R., Vescovo, L., Gianelle, D., Sims, D.A., Rahman, A.F., Pastorello, G.Z., 2010. SpecNet revisited: bridging flux and remote sensing communities. Can. J. Remote Sens. 36, S376–S390. http://dx.doi.org/10.5589/m10-067.

Gamon, J.A., Huemmrich, K.F., Wong, C.Y.S., Ensminger, I., Garrity, S., Hollinger, D.Y., Noormets, A., Peñuelas, J., 2016. A remotely sensed pigment index reveals photosynthetic phenology in evergreen conifers. PNAS 113, 13087–13092. http://dx.doi.org/10.1073/pnas.1606162113.

Garbulsky, M.F., Peñuelas, J., Papale, D., Filella, I., 2008. Remote estimation of carbon dioxide uptake by a Mediterranean forest. Global Change Biol. 14, 2860–2867. http://dx.doi.org/10.1111/j.1365-2486.2008.01684.x.

Goulden, M.L., Anderson, R.G., Bales, R.C., Kelly, A.E., Meadows, M., Winston, G.C., 2012. Evapotranspiration along an elevation gradient in California's Sierra Nevada. J. Geophys. Res. G: Biogeosci. 117.

Granier, A., 1987. Evaluation of transpiration in a Douglas-fir stand by means of sap flow measurements. Tree Physiol. 3, 309–320.

Granier, A., 1985. Une nouvelle méthode pour la mesure du flux de sève brute dans le tronc des arbres. Ann. For. Sci. 42, 193–200. http://dx.doi.org/10.1051/forest:19850204.

Groffman, P.M., Driscoll, C.T., Fahey, T.J., Hardy, J.P., Fitzhugh, R.D., Tierney, G.L., 2001. Colder soils in a warmer world: A snow manipulation study in a northern hardwood forest ecosystem. Biogeochemistry 56, 135–150.

Gutmann, E.D., Van Stan II, J.T., Friesen, J., Aubrey, D.P., Lundquist, J., 2017. Observed compression of in situ tree stems during freezing. Agric. For. Meteorol. 243, 19–24. http://dx.doi.org/10.1016/j.agrformet.2017.05.004.

Hadley, J.L., 2000. Effect of daily minimum temperature on photosynthesis in Eastern Hemlock (Tsuga canadensis L.) in autumn and winter. Arct., Antarctic, Alp. Res. 32, 368–374. http://dx.doi.org/10.2307/1552384.

Hamlet, A.F., Mote, P.W., Clark, M.P., Lettenmaier, D.P., 2005. Effects of temperature and precipitation variability on snowpack trends in the Western United States. J. Clim. 18, 4545–4561.

Hu, J., Moore, D.J.P., Riveros-Iregui, D.A., Burns, S.P., Monson, R.K., 2010. Modeling whole-tree carbon assimilation rate using observed transpiration rates and needle sugar carbon isotope ratios. New Phytol. 185, 1000–1015.

Huxman, T.E., Turnipseed, A.A., Sparks, J.P., Harley, P.C., Monson, R.K., 2003. Temperature as a control over ecosystem CO2 fluxes in a high-elevation, subalpine forest. Oecologia 134, 537–546. http://dx.doi.org/10.1007/s00442-002-1131-1.

Jahns, P., Holzwarth, A.R., 2012. The role of the xanthophyll cycle and of lutein in photoprotection of photosystem II. Biochim. et Biophys. Acta (BBA) – Bioenerg., Photosyst. II 1817, 182–193. http://dx.doi.org/10.1016/j.bbabio.2011.04.012.

Jeong, S.-J., Schimel, D., Frankenberg, C., Drewry, D.T., Fisher, J.B., Verma, M., Berry, J.A., Lee, J.-E., Joiner, J., 2017. Application of satellite solar-induced chlorophyll fluorescence to understanding large-scale variations in vegetation phenology and function over northern high latitude forests. Remote Sens. Environ. 190, 178–187. http://dx.doi.org/10.1016/j.rse.2016.11.021.

Jia, Y., Shelhamer, E., Donahue, J., Karayev, S., Long, J., Girshick, R., Guadarrama, S., Darrell, T., 2014. Caffe: convolutional architecture for fast feature embedding. In: Proceedings of the 22Nd ACM International Conference on Multimedia, MM '14. ACM, New York, NY, USA. pp. 675–678. http://dx.doi.org/10.1145/2647868.2654889.

Kapnick, S., Hall, A., 2012. Causes of recent changes in western North American snowpack. Clim. Dyn 38, 1885–1899. http://dx.doi.org/10.1007/s00382-011-1089-y.

Kaufmann, M.R., 1975. Leaf water stress in Engelmann spruce. Plant Physiol. 56, 841–844.

Keenan, T.F., Darby, B., Felts, E., Sonnentag, O., Friedl, M.A., Hufkens, K., O'Keefe, J., Klosterman, S., Munger, J.W., Toomey, M., Richardson, A.D., 2014. Tracking forest phenology and seasonal physiology using digital repeat photography: a critical assessment. Ecol. Appl. 24, 1478–1489. http://dx.doi.org/10.1890/13-0652.1.

Kim, Y., Still, C.J., Hanson, C.V., Kwon, H., Greer, B.T., Law, B.E., 2016. Canopy skin

temperature variations in relation to climate, soil temperature, and carbon flux at a ponderosa pine forest in central Oregon. Agric. For. Meteorol. 226–227, 161–173. http://dx.doi.org/10.1016/j.agrformet.2016.06.001.
Kittel, T.G.F., Williams, M.W., Chowanski, K., Hartman, M., Ackerman, T., Losleben, M., Blanken, P.D., 2015. Contrasting long-term alpine and subalpine precipitation trends in a mid-latitude North American mountain system, Colorado Front Range, USA. Plant Ecol. Diver. 8, 607–624. http://dx.doi.org/10.1080/17550874.2016.1143536.
Knowles, N., Dettinger, M.D., Cayan, D.R., 2006. Trends in snowfall versus rainfall in the Western United States. J. Clim. 19, 4545–4559.
Kolari, P., Chan, T., Porcar-Castell, A., Bäck, J., Nikinmaa, E., Juurola, E., 2014. Field and controlled environment measurements show strong seasonal acclimation in photosynthesis and respiration potential in boreal Scots pine. Front. Plant Sci. 5, 717. http://dx.doi.org/10.3389/fpls.2014.00717.
Kreyling, J., 2010. Winter climate change: a critical factor for temperate vegetation performance. Ecology 91, 1939–1948.
Leuzinger, S., Körner, C., 2007. Tree species diversity affects canopy leaf temperatures in a mature temperate forest. Agric. Forest Meteorol. 146, 29–37. http://dx.doi.org/10.1016/j.agrformet.2007.05.007.
Liu, X., Nie, Y., Luo, T., Yu, J., Shen, W., Zhang, L., 2016. Seasonal shift in climatic limiting factors on tree transpiration: evidence from sap flow observations at Alpine Treelines in Southeast Tibet. Front. Plant Sci. 7. http://dx.doi.org/10.3389/fpls.2016.01018.
Mark, W.R., Crews, D.L., 1973. Heat-pulse velocity and bordered pit condition in living Engelmann spruce and lodgepole pine trees. For. Sci. 19, 291–296.
Matheny, A.M., Mirfenderesgi, G., Bohrer, G., 2017. Trait-based representation of hydrological functional properties of plants in weather and ecosystem models. Plant Divers. 39, 1–12. http://dx.doi.org/10.1016/j.pld.2016.10.001.
Maurer, G.E., Bowling, D.R., 2014. Seasonal snowpack characteristics influence soil temperature and water content at multiple scales in interior western U.S. mountain ecosystems. Water Resour. Res. 50, 5216–5234. http://dx.doi.org/10.1002/2013WR014452.
Mayr, S., Charra-Vaskou, K., 2007. Winter at the alpine timberline causes complex within-tree patterns of water potential and embolism in Picea abies. Physiol. Plant. 131, 131–139. http://dx.doi.org/10.1111/j.1399-3054.2007.00942.x.
Mayr, S., Schmid, P., Laur, J., Rosner, S., Charra-Vaskou, K., Dämon, B., Hacke, U.G., 2014. Uptake of water via branches helps timberline conifers refill embolized xylem in late winter. Plant Physiol. 164, 1731–1740. http://dx.doi.org/10.1104/pp.114.236646.
Mayr, S., Schwienbacher, F., Bauer, H., 2003. Winter at the alpine timberline. Why does embolism occur in Norway spruce but not in Stone pine? Plant Physiol. 131, 780–792. http://dx.doi.org/10.1104/pp.011452.
Mayr, S., Wieser, G., Bauer, H., 2006. Xylem temperatures during winter in conifers at the alpine timberline. Agric. Forest Meteorol. 137, 81–88. http://dx.doi.org/10.1016/j.agrformet.2006.02.013.
McGuire, C.R., Nufio, C.R., Bowers, M.D., Guralnick, R.P., 2012. Elevation-dependent temperature trends in the Rocky Mountain Front Range: changes over a 56- and 20-year record. PLoS One 7. http://dx.doi.org/10.1371/journal.pone.0044370.
Mitton, J., Ferrenberg, S.M., 2012. Mountain pine beetle develops an unprecedented summer generation in response to climate warming. Am. Nat. 179, 1–9.
Molotch, N.P., Blanken, P.D., Williams, M.W., Turnipseed, A.A., Monson, R.K., Margulis, S.A., 2007. Estimating sublimation of intercepted and sub-canopy snow using eddy covariance systems. Hydrol. Process. 21, 1567–1575. http://dx.doi.org/10.1002/hyp.6719.
Monson, R.K., Sparks, J.P., Rosenstiel, T.N., Scott-Denton, L.E., Huxman, T.E., Harley, P.C., Turnipseed, A.A., Burns, S.P., Backlund, B., Hu, J., 2005. Climatic influences on net ecosystem CO2 exchange during the transition from wintertime carbon source to springtime carbon sink in a high-elevation, subalpine forest. Oecologia 146, 130–147.
Monson, R.K., Turnipseed, A.A., Sparks, J.P., Harley, P.C., Scott-Denton, L.E., Sparks, K., Huxman, T.E., 2002. Carbon sequestration in a high-elevation, subalpine forest. Global Change Biol. 8, 459–478.
Moore, D.J.P., Hu, J., Sacks, W.J., Schimel, D.S., Monson, R.K., 2008. Estimating transpiration and the sensitivity of carbon uptake to water availability in a subalpine forest using a simple ecosystem process model informed by measured net CO2 and H2O fluxes. Agric. For. Meteorol. 148, 1467–1477.
Mote, P.W., Hamlet, A.F., Clark, M.P., Lettenmaier, D.P., 2005. Declining mountain snowpack in Western North America. Bull. Am. Meteorol. Soc. 86, 39–49.
Motohka, T., Nasahara, K.N., Oguma, H., Tsuchida, S., 2010. Applicability of green-red vegetation index for remote sensing of vegetation phenology. Remote Sens. 2, 2369–2387. http://dx.doi.org/10.3390/rs2102369.
Nippert, J.B., Duursma, R.A., Marshall, J.D., 2004. Seasonal variation in photosynthetic capacity of montane conifers. Funct. Ecol. Funct. Ecol. 18, 876–886.
Nogués-Bravo, D., Araújo, M.B., Errea, M.P., Martínez-Rica, J.P., 2007. Exposure of global mountain systems to climate warming during the 21st century. Global Environ. Change 17, 420–428. http://dx.doi.org/10.1016/j.gloenvcha.2006.11.007.
Oleson, et al., 2013. Technical Description of Version 4.5 of the Community Land Model (CLM).
Öquist, G., Huner, N.P.A., 2003. Photosynthesis of overwintering evergreen plants. Annu. Rev. Plant Biol. 54, 329–355. http://dx.doi.org/10.1146/annurev.arplant.54.072402.115741.
Pataki, D.E., Oren, R., Smith, W.K., 2000. Sap flux of co-occurring species in a western subalpine forest during seasonal soil drought. Ecology 81, 2557–2566.
Pederson, G.T., Betancourt, J.L., McCabe, G.J., 2013. Regional patterns and proximal causes of the recent snowpack decline in the Rocky Mountains, U.S. Geophys. Res. Lett. 40, 1811–1816. http://dx.doi.org/10.1002/grl.50424.
Piao, S., Wang, X., Ciais, P., Zhu, B., Wang, T., Liu, J., 2011. Changes in satellite-derived vegetation growth trend in temperate and boreal Eurasia from 1982 to 2006. Global Change Biol. 17, 3228–3239. http://dx.doi.org/10.1111/j.1365-2486.2011.02419.x.
Polgar, C.A., Primack, R.B., 2011. Leaf-out phenology of temperate woody plants: from trees to ecosystems. New Phytol. 191, 926–941. http://dx.doi.org/10.1111/j.1469-8137.2011.03803.x.
Porcar-Castell, A., 2011. A high-resolution portrait of the annual dynamics of photochemical and non-photochemical quenching in needles of Pinus sylvestris. Physiol. Plant 143, 139–153. http://dx.doi.org/10.1111/j.1399-3054.2011.01488.x.
Porcar-Castell, A., Garcia-Plazaola, J.I., Nichol, C.J., Kolari, P., Olascoaga, B., Kuusinen, N., Fernández-Marín, B., Pulkkinen, M., Juurola, E., Nikinmaa, E., 2012. Physiology of the seasonal relationship between the photochemical reflectance index and photosynthetic light use efficiency. Oecologia 170, 313–323. http://dx.doi.org/10.1007/s00442-012-2317-9.
Porcar-Castell, A., Tyystjärvi, E., Atherton, J., van der Tol, C., Flexas, J., Pfündel, E.E., Moreno, J., Frankenberg, C., Berry, J.A., 2014. Linking chlorophyll a fluorescence to photosynthesis for remote sensing applications: mechanisms and challenges. J. Exp. Bot. 65, 4065–4095. http://dx.doi.org/10.1093/jxb/eru191.
Raczka, B., Duarte, H.F., Koven, C.D., Ricciuto, D., Thornton, P.E., Lin, J.C., Bowling, D.R., 2016. An observational constraint on stomatal function in forests: evaluating coupled carbon and water vapor exchange with carbon isotopes in the community land model (CLM4.5). Biogeosciences 13, 5183–5204. http://dx.doi.org/10.5194/bg-13-5183-2016.
Reichstein, M., Falge, E., Baldocchi, D., Papale, D., Aubinet, M., Berbigier, P., Bernhofer, C., Buchmann, N., Gilmanov, T., Granier, A., Grunwald, T., Havrankova, K., Ilvesniemi, H., Janous, D., Knohl, A., Laurila, T., Lohila, A., Loustau, D., Matteucci, G., Meyers, T., Miglietta, F., Ourcival, J.M., Pumpanen, J., Rambal, S., Rotenberg, E., Sanz, M., Tenhunen, J., Seufert, G., Vaccari, F., Vesala, T., Yakir, D., Valentini, R., 2005. On the separation of net ecosystem exchange into assimilation and ecosystem respiration: review and improved algorithm. Global Change Biol. 11, 1424–1439.
Richardson, A.D., Black, T.A., Ciais, P., Delbart, N., Friedl, M.A., Gobron, N., Hollinger, D.Y., Kutsch, W.L., Longdoz, B., Luyssaert, S., Migliavacca, M., Montagnani, L., Munger, J.W., Moors, E., Piao, S., Rebmann, C., Reichstein, M., Saigusa, N., Tomelleri, E., Vargas, R., Varlagin, A., 2010. Influence of spring and autumn phenological transitions on forest ecosystem productivity. Phil. Trans. R. Soc. B : Biol. Sci. 365, 3227–3246.
Richardson, A.D., Hollinger, D.Y., 2005. Statistical modeling of ecosystem respiration using eddy covariance data: maximum likelihood parameter estimation, and Monte Carlo simulation of model and parameter uncertainty, applied to three simple models. Agric. For. Meteorol. 131, 191–208. http://dx.doi.org/10.1016/j.agrformet.2005.05.008.
Richardson, A.D., Hollinger, D.Y., Dail, D.B., Lee, J.T., Munger, J.W., O'keefe, J., 2009. Influence of spring phenology on seasonal and annual carbon balance in two contrasting New England forests. Tree Physiol. 29, 321–331. http://dx.doi.org/10.1093/treephys/tpn040.
Running, S.W., Reid, C.P., 1980. Soil temperature influences on root resistance of Pinus contorta seedlings. Plant Physiol. 65, 635–640. http://dx.doi.org/10.1104/pp.65.4.635.
Ryan, M.G., 1989. Sapwood volume for three subalpine conifers: predictive equations and ecological implications. Can. J. For. Res. 19, 1397–1401. http://dx.doi.org/10.1139/x89-214.
Scalzitti, J., Strong, C., Kochanski, A., 2016. Climate change impact on the roles of temperature and precipitation in Western U.S. snowpack variability. Geophys. Res. Lett. 43, GL068798. http://dx.doi.org/10.1002/2016GL068798.
Schaberg, P.G., Shane, J.B., Cali, P.F., Donnelly, J.R., Strimbeck, G.R., 1998. Photosynthetic capacity of red spruce during winter. Tree Physiol. 18, 271–276. http://dx.doi.org/10.1093/treephys/18.4.271.
Schulze, E.D., Mooney, H.A., Dunn, E.L., 1967. Wintertime photosynthesis of bristlecone pine (Pinus Aristata) in the White Mountains of California. Ecology 48, 1044–1047. http://dx.doi.org/10.2307/1934564.
Sevanto, S., Suni, T., Pumpanen, J., GrÃnholm, T., Kolari, P., Nikinmaa, E., Hari, P., Vesala, T., 2006. Wintertime photosynthesis and water uptake in a Boreal forest. Tree Physiol. 26, 749–757.
Sonnentag, O., Hufkens, K., Teshera-Sterne, C., Young, A.M., Friedl, M., Braswell, B.H., Milliman, T., O'Keefe, J., Richardson, A.D., 2012. Digital repeat photography for phenological research in forest ecosystems. Agric. For. Meteorol. 152, 159–177. http://dx.doi.org/10.1016/j.agrformet.2011.09.009.
Sparks, J.P., Campbell, G.S., Black, R.A., 2001. Water content, hydraulic conductivity, and ice formation in winter stems of Pinus contorta: a TDR case study. Oecologia 127, 468–475.
Sperry, J.S., Nichols, K.L., Sullivan, J.E.M., Eastlack, S.E., 1994. Xylem embolism in ring-porous, diffuse-porous, and coniferous trees of Northern Utah and Interior Alaska. Ecology 75, 1736–1752. http://dx.doi.org/10.2307/1939633.
Sperry, J.S., Wang, Y., Wolfe, B.T., Mackay, D.S., Anderegg, W.R.L., McDowell, N.G., Pockman, W.T., 2016. Pragmatic hydraulic theory predicts stomatal responses to climatic water deficits. New Phytol. 212, 577–589. http://dx.doi.org/10.1111/nph.14059.
Steltzer, H., Landry, C., Painter, T.H., Anderson, J., Ayres, E., 2009. Biological consequences of earlier snowmelt from desert dust deposition in alpine landscapes. Proc. Natl. Acad. Sci. U. S. A. 106, 11629–11634.
Stewart, I.T., Cayan, D.R., Dettinger, M.D., 2005. Changes toward earlier streamflow timing across Western North America. J. Clim. 18, 1136–1155.
Tucker, C.J., 1979. Red and photographic infrared linear combinations for monitoring vegetation. Remote Sens. Environ. 8, 127–150. http://dx.doi.org/10.1016/0034-4257(79)90013-0.
Turcotte, A., Morin, H., Krause, C., Deslauriers, A., Thibeault-Martel, M., 2009. The timing of spring rehydration and its relation with the onset of wood formation in black spruce. Agric. For. Meteorol. 149, 1403–1409. http://dx.doi.org/10.1016/j.

agrformet.2009.03.010.
Vandegehuchte, M.W., Steppe, K., 2013. Sap-flux density measurement methods: working principles and applicability. Funct. Plant Biol. 40, 213–223.
Verhoeven, A., 2014. Sustained energy dissipation in winter evergreens. New Phytol. 201, 57–65. http://dx.doi.org/10.1111/nph.12466.
Walther, S., Voigt, M., Thum, T., Gonsamo, A., Zhang, Y., Köhler, P., Jung, M., Varlagin, A., Guanter, L., 2016. Satellite chlorophyll fluorescence measurements reveal large-scale decoupling of photosynthesis and greenness dynamics in boreal evergreen forests. Global Change Biol. 22, 2979–2996. http://dx.doi.org/10.1111/gcb.13200.
Winchell, T.S., Barnard, D.M., Monson, R.K., Burns, S.P., Molotch, N.P., 2016. Earlier snowmelt reduces atmospheric carbon uptake in midlatitude subalpine forests. Geophys. Res. Lett. GL069769. http://dx.doi.org/10.1002/2016GL069769.
Wingate, L., Ogée, J., Cremonese, E., Filippa, G., Mizunuma, T., Migliavacca, M., Moisy, C., Wilkinson, M., Moureaux, C., Wohlfahrt, G., Hammerle, A., Hörtnagl, L., Gimeno, C., Porcar-Castell, A., Galvagno, M., Nakaji, T., Morison, J., Kolle, O., Knohl, A., Kutsch, W., Kolari, P., Nikinmaa, E., Ibrom, A., Gielen, B., Eugster, W., Balzarolo, M., Papale, D., Klumpp, K., Köstner, B., Grünwald, T., Joffre, R., Ourcival, J.-M., Hellstrom, M., Lindroth, A., George, C., Longdoz, B., Genty, B., Levula, J., Heinesch, B., Sprintsin, M., Yakir, D., Manise, T., Guyon, D., Ahrends, H., Plaza-Aguilar, A., Guan, J.H., Grace, J., 2015. Interpreting canopy development and physiology using a European phenology camera network at flux sites. Biogeosciences 12, 5995–6015. http://dx.doi.org/10.5194/bg-12-5995-2015.
Wong, C.Y.S., Gamon, J.A., 2015a. The photochemical reflectance index provides an optical indicator of spring photosynthetic activation in evergreen conifers. New Phytol. 206, 196–208. http://dx.doi.org/10.1111/nph.13251.
Wong, C.Y.S., Gamon, J.A., 2015b. Three causes of variation in the photochemical reflectance index (PRI) in evergreen conifers. New Phytol. 206, 187–195. http://dx.doi.org/10.1111/nph.13159.
Xu, X., Medvigy, D., Powers, J.S., Becknell, J.M., Guan, K., 2016. Diversity in plant hydraulic traits explains seasonal and inter-annual variations of vegetation dynamics in seasonally dry tropical forests. New Phytol. 212, 80–95. http://dx.doi.org/10.1111/nph.14009.
Zhang, T., Barry, R.G., Armstrong, R.L., 2004. Application of satellite remote sensing techniques to frozen ground studies. Polar Geogr. 28, 163–196. http://dx.doi.org/10.1080/789610186.
Zhou, B., Lapedriza, A., Xiao, J., Torralba, A., Oliva, A., 2014. Learning deep features for scene recognition using places database. In: Ghahramani, Z., Welling, M., Cortes, C., Lawrence, N.D., Weinberger, K.Q. (Eds.), Advances in Neural Information Processing Systems 27. Curran Associates, Inc., pp. 487–495.
Zwieniecki, M.A., Holbrook, N.M., 2009. Confronting Maxwell's demon: biophysics of xylem embolism repair. Trends Plant Sci. 14, 530–534. http://dx.doi.org/10.1016/j.tplants.2009.07.002.